Research Article

Microbial Consortia from Chilean Salt Flats Drive Coupled Gypsum Dissolution and Mineralization in the Absence of Evaporation: Experimental Evidence

Ivan Orellana[1,2], Cinthya Tebes[1,2], Cecilia Demergasso[2], Óscar Cabestrero[3,2]

1. Departamento de Ciencias Geológicas, Facultad de Ingeniería y Ciencias Geológicas, Universidad Catolica del Norte, Chile; 2. Centro de Biotecnología Alberto Ruíz, Universidad Catolica del Norte, Chile; 3. Departamento de Mineralogía y Petrología, Facultad de Ciencias Geológicas, Universidad Complutense de Madrid, Spain

Microbial consortia actively modulate mineralogical processes in polyextreme environments, yet biological mechanisms are often excluded from evaporite evolution models. Here, we investigated gypsum surface dissolution and secondary mineral nucleation driven by microbial mats and natural brines from three Andean salt flats (Salar de Llamara, Salar de Pajonales, and Salar de Gorbea) across 90-day incubation experiments. Synthesized gypsum crystals were exposed to inoculated media and sterile brines (abiotic controls) under controlled conditions, and analyzed using SEM-EDS and epifluorescence microscopy. Results demonstrate that microbial colonization dual-modulates gypsum dynamics: while apparent microbially-mediated boring formed rounded cavities, extracellular polymeric substance (EPS) matrices acted as diffusion barriers that buffered abiotic dissolution. Furthermore, EPS promoted localized supersaturation and authigenic mineral nucleation, yielding fibrous eugsterite and globular Mg-silicates across all sites, alongside site-specific phases such as dumbbell-shaped calcite, allotriomorphic halite (Pajonales), and lenticular alunite (Gorbea). Abiotic controls exhibited simpler parageneses and angular dissolution along cleavage planes without filling. Specific bio-induced textures, including EPS-infilled pores, dumbbell calcite, Mg-Si globules, and alveolar eugsterite, represent potential morphological biosignatures relevant to astrobiology. Our findings demonstrate that purely abiotic geochemical models are insufficient to describe brine evolution, underscoring the critical necessity of integrating geomicrobiological interactions into evaporite formation frameworks.

 doi.org/10.32388/ED4EYH.3

Corresponding author: Iván D. Orellana-Villota, i.orellanavillota@gmail.com

1. Introduction

Evaporitic environments have long been recognized as archives of hydrological and geochemical processes[1][2] (Hardie et al., 1978). In northern Chile, these environments known as salt flats represent polyextreme habitats that function as true centers of biodiversity that has adapted to high UV radiation, low water availability and high salt concentration. Within this desert zone, high salinity provide thermodynamically beneficial conditions for the proliferation of highly specialized microbiota[3][4][5][6]. The profound nature of these ecosystems is even reflected in local traditions, which ancestrally consider them the very cradle of life. Beyond their cultural and geological relevance, these polyextreme systems serve as natural laboratories for biosignature preservation, as mineral precipitation often traps evidence of life. In particular, evaporitic minerals like gypsum play a central role in the preservation of microbe-mineral assemblages, biosignatures and textures under extreme conditions[7][8]. This preservation potential is a globally recognized phenomenon observed across both modern and ancient evaporitic settings. For instance, microbially mediated calcium sulfate precipitation has been widely documented in various geographic contexts, ranging from the hyper-saline microbial mats of Baja California to the ephemeral lakes of Central Spain, highlighting the global scale of the role of biogeochemical brine evolution and evaporate formation in biosignature preservation[9][10][11].

Despite these observations, most conceptual models of evaporite formation have historically emphasized abiotic factors, focusing on hydrological balance and geochemical saturation while leaving microbial influences largely unaddressed. This gap between evidence of microbe–mineral interactions modelling mineral nucleation and the prevailing geochemical frameworks highlights the need for evidence that supports the integration of biological processes in evaporite formation models.

1.1. Evaporitic Deposits, Geological Setting and Microbial Communities

Traditionally, evaporite deposit formation in salt flats is attributed to ion concentration[12][13][1][14], with salt crust dynamics reflecting water balance and recharge regimes[15][16]. Within northern Chile, the Atacama Desert and the Altiplano-Puna plateau host diverse salt flats that illustrate a physicochemical contrast, with hyper-acidic to alkaline pH, and subsaline to hypersaline brines driven by complex hydrogeochemistry[17][15][16][18]. Moreover, they also display different geological settings, high thermal oscillation, high evaporation rates, and low to absent rainfall. In these environments. microbe-mineral

structures ranging from biofilm-rich muds to complex microbial mats, endoevaporites and stromatolites are found, and are subjected to the extreme and evolving environmental conditions[3][19][5][8]

Among the studied salt flats (Figure 1b-c), Salar de Llamara, in the Central Depression at around 800 m.a.s.l., is characterized by shallow brines (pH 7.0–8.3) with a high salinity gradient (10-300 g L^{-1} NaCl), sulfate- and chloride-rich deposits, and limited recharge, favoring extensive gypsum/halite crusts with lesser carbonates and fossilized microbial mats[2][5][17]. On the other hand, Salar de Pajonales (Figure 1d-e), at 3517 m.a.s.l. in the High Andes, is sustained by snowmelt, rainfall, and groundwater discharge. Pajonales represents a hypersaline, neutro-alkaline (pH 6.5-8.5) system with a wide salinity gradient (4–390 g L^{-1} NaCl). Its mineralogy is dominated by gypsum ($CaSO_4{\cdot}2H_2O$), halite (NaCl), calcite ($CaCO_3$), anhydrite ($CaSO_4$), and glauberite ($Na_2Ca(SO_4)_2$)[20][21][8]. Salar de Gorbea (Figure 1f-g), further south at 3950 m.a.s.l., represents a hydrothermal-influenced basin with extremely acidic, moderately saline brines (pH 1.7–4.2; 10–60 g L^{-1} NaCl). Here, sulfates (mostly gypsum), native sulfur, halite, and alunite ($KAl_3(SO_4)_2(OH)_6$) form under polyextreme conditions. Other common mineral assemblages include thenardite (Na_2SO_4), carnallite ($KMgCl_3{\cdot}6H_2O$), epsomite ($MgSO_4{\cdot}7H_2O$), and starkeyite ($MgSO_4{\cdot}4H_2O$), with trace amounts of kainite ($KMg(SO_4)\ Cl{\cdot}3H_2O$), tachyhydrite ($CaMg_2Cl_6{\cdot}12H_2O$), Mg-aubertite ($MgAl_2(SO_4)_4{\cdot}22H_2O$), and jarosite ($KFe_3(SO_4)_2(OH)_6$)[6][22][18][8].

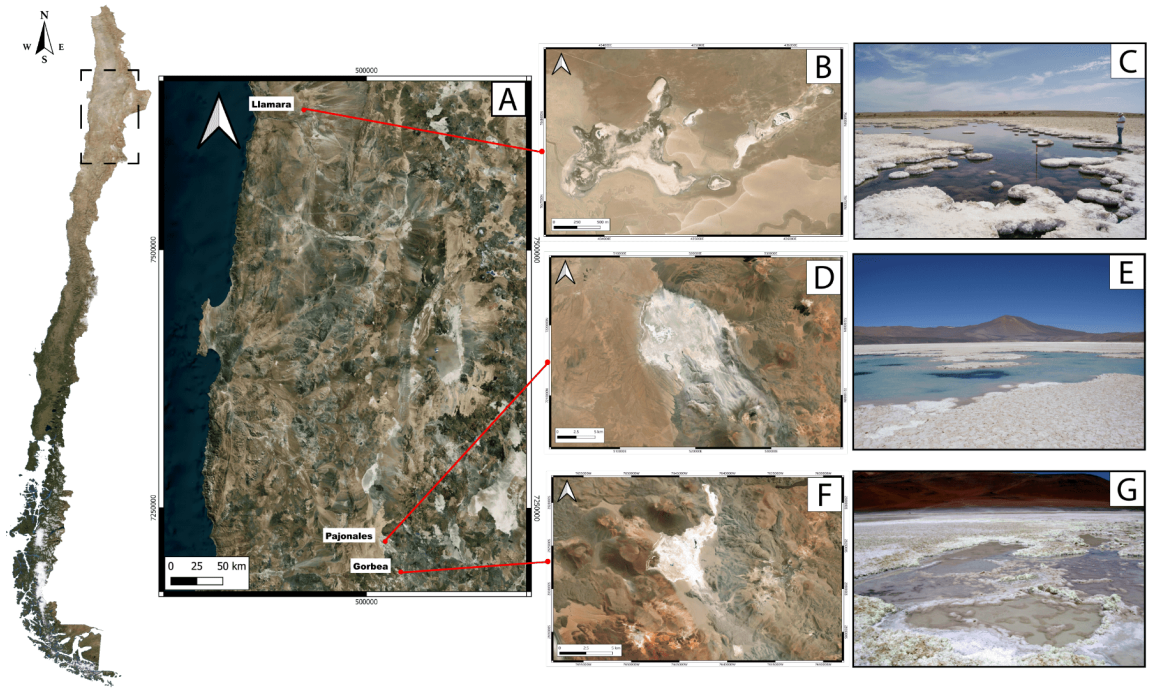


Figure 1. Geographic location of salt flats from which microbial mats and brines were collected. A) Location of the studied salt flats among many other salt flats present in the area, which are seen with lighter colored basins surrounded mainly by volcanic outcrops and mountain ranges in darker colors which are visible due to the absence of vegetation. B) Salar de Llamara with its 4 *puquios* and small ponds in the transition zone between main water bodies. (C) Characteristic domical gypsum formations found in Salar de Llamara. D) Salar de Pajonales located between gravel-covered volcanic rocks to the west, and cretacic lava flows next to volcanoes to the east. (E) Light blue to deep blue brines from Salar de Pajonales surrounded by gypsum. (F) Salar de Gorbea surrounded by volcanoes and alluvial fans, as well as Salar Ignorado to the south. (G) Characteristic yellow Al/Mg(Fe) sulfate-covered gypsum crust of Salar de Gorbea.

Beyond hydrochemistry and sedimentology, microbial communities in these salt flats comprise a fundamental part of the environments, and, by microbe-mineral interactions biogeochemical processes may be modulated. For instance, these interactions may take place in LLA due to microbial communities that dominated by diatoms, Cyanobacteriota, Pseudomonadota, and sulfate-reducing bacteria[3][5]. On the other hand, PAJ gypsum deposits host microbial communities dominated by Cyanobacteriota, Pseudomonadota, Actinobacteriota, Bacteroidota, and Chloroflexota[21][23][8]. In contrast, GOR gypsum microbial communities are adapted to extreme acidity and sulfate concentration, including Bacillota, Pseudomonadota, and Actinobacteriota[24]. Additionally, mixotrophic taxa such as Leifsonia and

Novosphingobium, which capable of metal and sulfur redox transformations, have been identified in GOR[24][22][25].

1.2. Microbe-mineral Interactions in Evaporites

Microorganisms influence mineralization through several mechanisms: they generate distinctive textures such as rosettes, framboids, and alveolar or radiating arrangements, among others[9][6][26][27][19][28]; and they produce isotopic signatures that deviate from equilibrium with ambient waters[29][30]. Crucially, microorganisms actively secrete exopolymeric substances (EPS) and other organic metabolites that locally modulate pH and ion availability. These organic excretions not only create chemical gradients that facilitate mineral nucleation, but they also heavily influence crystal growth and, consequently, the resulting crystal morphology. For instance, specific organic molecules have been shown to drive crystal dissolution and produce irregular habits, such as abnormally equant gypsum crystals[31]. On the other hand, Nicoleau et al.[32] demonstrated that industrial polymers (similar to those in EPS) delay gypsum nucleation via a kinetics-based mechanism that hinders the collision and merging of primary mineral species, effectively overriding their thermodynamic effect of stabilizing the crystal-solution interface.

The macroscopic manifestations of microbe-mineral interactions can be seen across a spectrum of sedimentary and geobiological structures representing distinct stages of lithification and layering driven both by abiotic and biomineralization processes. These range from biofilm-rich loose sediments and microbial mats with characteristic layering and different degrees of lithification, to heavily lithified and structurally complex microbialites[3][5]. Beyond influencing mineral precipitation and sediment stabilization, microorganisms actively exploit these mineralized matrices as a primary habitat, representing a distinct and critical form of microbe-mineral interaction. In the hyperarid and high-altitude settings of the Atacama Desert, evaporitic crusts provide protection from the harsh conditions on the surface. Due to its specific physicochemical properties, gypsum emerges as a privileged substrate for this endolithic lifestyle. Its unique optical properties allow photosynthetically active radiation to penetrate while effectively filtering out a substantial amount of UV radiation, creating a protected, thermodynamically stable microenvironment[33][34]. Furthermore, the porous architecture of the gypsum matrix helps retain moisture under hyperarid conditions[35][36][37]. Moreover, the presence of diatoms and other phototrophs in fluid inclusions within evaporite crystals has been previously reported in PAJ and GOR[38]. On the other hand, the extraction of the molecular water contained in gypsum's crystalline structure by endolithic activity has been proposed by other authors. For instance, Wang et al.

[39] reported the phase change from calcium sulfate di-hydrate (gypsum) to anhydrous calcium sulfate (anhydrite) and proposed that microbes preferably colonize cleavage planes to have access to molecular water. Consequently, endolithic colonization of these gypsum structures has been widely reported, with cyanobacteria and other highly specialized microbiota migrating within the mineral matrix in response to light intensity[40][41]. Inside these rocks, they organize into distinct stratified communities, producing protective pigments and metabolites to survive[42][43][37]. For these reasons, understanding the dynamics of this endolithic colonization is highly relevant: just as microbial activity influences mineralization, the physiological adaptations of endolithic communities actively alter and modulate pre-existing minerals, influencing overall brine and evaporite evolution while leaving behind biosignatures and textures preserved in the geological record.

The geobiological setting of the salt flats considered in this study is characterized by a complex interplay between biological activity, water chemistry, and sedimentology. In Salar de Llamara, for instance, electrical conductivity gradients modulate both microbial diversity and sediment composition: lower conductivity favors carbonate-dominated sediments and diverse microbial communities, whereas higher conductivity leads to sulfate-halide assemblages and reduced microbial diversity[5]. On the other hand, experiments with natural microbial consortia from Pajonales and Gorbea were conducted by Cabestrero et al.[6] under controlled laboratory conditions with intact mats and natural brines. Their research demonstrated that community activity can induce gypsum, halite, calcite and magnesium-rich silicate precipitation even in undersaturated conditions, without evaporation. These findings emphasize the collective role of Andean salt flat microbial consortia in driving mineralization processes beyond purely abiotic controls or isolated microorganisms in ideal conditions.

Importantly, understanding these specific microbe-gypsum interactions is not only fundamental for accurately modeling brine and evaporite evolution, but it also provides critical analogues for astrobiology and paleoclimatology[44]. Because gypsum can entomb cells, organic molecules, and fluid inclusions over geological timescales, identifying the specific morphological and isotopic biosignatures left by these extremophiles offers a blueprint for detecting ancient life in Martian sulfate deposits or reconstructing past terrestrial climates[45][46]. However, despite the astrobiological and paleoenvironmental significance of these biosignatures, microbial involvement in gypsum mineralization and dissolution remains poorly understood compared to carbonate systems[47][48]

Our limited understanding of these complex natural processes is in part the result of most previous laboratory studies relying on synthetic brines or isolated strains[49][50][51], which are limited in their ability to fully represent natural synergistic processes happening in gypsum-microbe arrangements. More recent work emphasizes the need to study microbial communities as complex, interacting systems under realistic biogeochemical conditions[6]. In this study, we aimed to differentiate textural and mineralogical changes induced by microbial consortia from those resulting purely from abiotic processes, focusing specifically on how EPS-producing microbes, such as cyanobacteria, modulate gypsum dissolution and the precipitation of secondary mineral phases that can result in biosignatures. Consequently, the main objective of this study is to evaluate and quantify textural changes in gypsum surface happening over time as a result of microbial activity, as well as identifying and characterizing mineral assemblages forming mostly through biomineralization processes. These textures and assemblages are then compared to their abiotic counterparts in order to specify the crucial role of microbial activity in mineral transformations.

2. Materials and Methods

A combination of geological and microbiological techniques was employed to monitor microbial changes in gypsum texture during time-controlled experiments (Fig. 2). Whole microbial mat samples, along with their corresponding water collected previously between 2018 and 2020[6] underwent a selection process prior to experimentation. Texture and morphology alterations in gypsum crystals and geomicrobiological interactions were analyzed using scanning electron microscopy with energy-dispersive X-ray spectroscopy (SEM-EDS). Microbial communities, on the other hand, were monitored with optical and fluorescence microscopy. Control experiments with uninoculated gypsum incubations were analyzed in parallel using the same techniques to discern abiotic changes. Additionally, autoclaved brine samples from each salt flat were also observed using optical microscopy to assess mineral presence prior to culture experimentation.

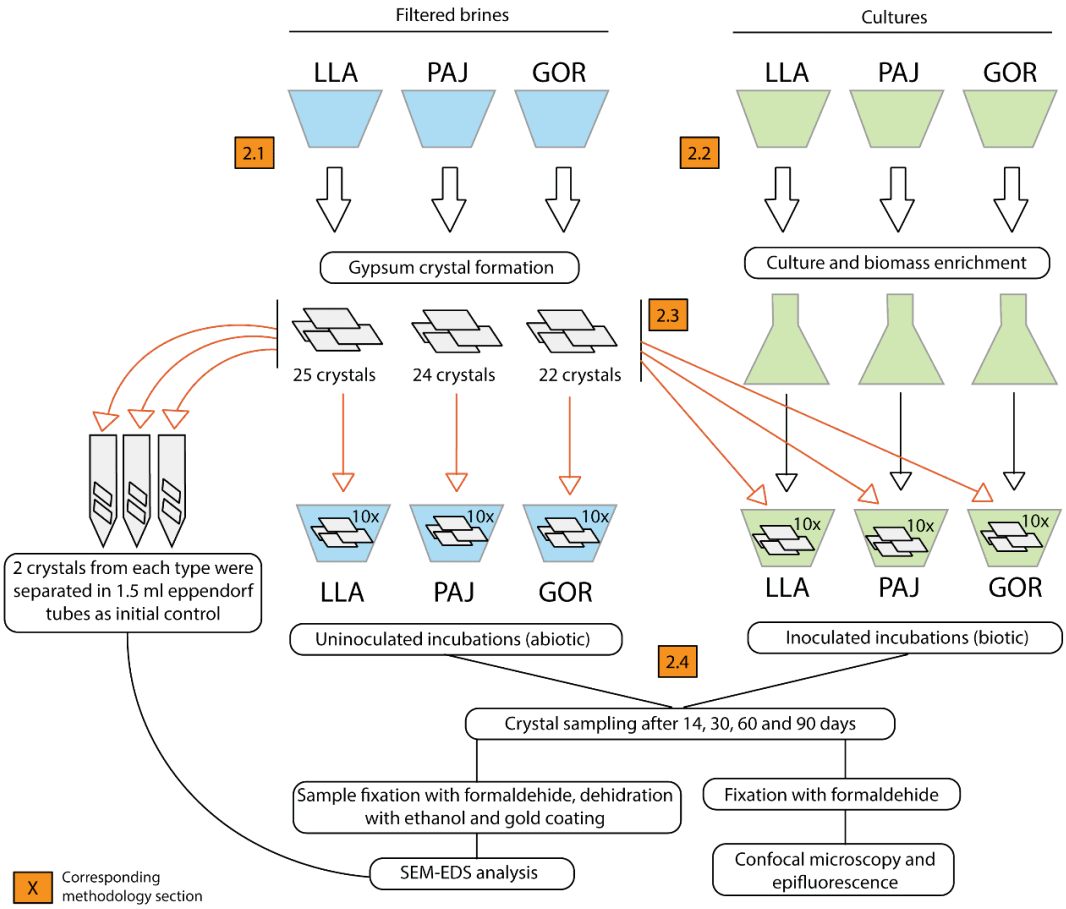


Figure 2. Flowchart illustrating the experimental design and step-by-step process. Step 1 (Section 2.1) selected filtered brines from Salar de Llamará (LLA), Salar de Pajonales (PAJ) and Salar de Gorbea (GOR) were evaporated to obtain gypsum crystals for experimentation. In parallel, BG-11-enriched cultures using intact microbial mat samples with their corresponding water was performed to obtain biomass for inoculation (Section 2.2). Then, crystals were placed inside containers with uninoculated and inoculated microcosms, respectively, while keeping two crystals from each salt flat intact as control (Section 2.3). Crystals were sampled after 14, 30, 60 and 90 days for SEM-EDS and epifluorescence microscopy (Section 2.4).

2.1. Water Sample Selection and Gypsum Crystal Growth

Water samples collected during the campaigns were sequentially filtered through 3 µm and 0.22 µm pore-size filters (Millipore, Burlington, MA, USA) to remove particles and microorganisms. The filtered water was then stored in sterilized plastic containers treated with 80% ethanol until used in the experiments.

doi.org/10.32388/ED4EYH.3

Sample selection was based on the gypsum saturation index calculated for brines prior to evaporation using PhreeQC with the Pitzer (LLA and PAJ) and Lnll (GOR) databases[52]. Samples that showed close to supersaturation for gypsum were selected for the following process. To obtain gypsum crystals for experimentation, 200 mL of selected water samples from the three studied salt flats were filtered through 0.22 µm pore size nitrocellulose filters and placed in open cylindrical glass containers for 2 months. Gypsum crystals were collected periodically as the water evaporated, using plastic coated tweezers and binocular lenses. Gypsum crystal selection involved identifying 10 well-formed crystals measuring 20 mm in length. Crystals were examined using a smartphone camera mounted on a 3D-printed plastic holder for binocular lenses.

2.2. Microbial Mat Manipulation, Culturing and Monitoring

Whole microbial mat samples from field campaigns were kept in glass containers with their corresponding water and gypsum substrate at 25°C with 12 hours of light daily in a closed aerobic chamber without agitation[6]. Some microbial mats were well consolidated (PAJ and LLA), with bubbles across the whole mat and even suspended in the water due to the accumulation of gases inside the mat, which caused the detachment. On the other hand, the rest of the samples were semi-consolidated and did not present an ideal microbial mat structure (visible layering) and were partially embedded in EPS (GOR).

To obtain more biomass prior experimentation, three samples from LLA, two from PAJ and a sample from GOR were selected from Cabestrero et al.[6] cultures. Microbial mats were then subsampled from their original containers using sterile tweezers and the subsamples were placed in 1.5 mL Eppendorf tubes. Subsequently, the tubes were subjected to a bath sonicator (Elmasonic S 30 H) to remove precipitates, disaggregate the samples, and detach cells adhered to mineral surfaces. After sonication, detached and suspended cells were transferred to 500 mL sterile flasks.

Prior to the experiment, to promote cyanobacterial growth and enhance biomass production, the inoculum (10^7 cells/mL) was introduced into 200 mL of culture medium, consisting of BG11 medium (Sigma C3061) at a 1:50 ratio with artificial brine (100 g/L NaCl). The pH was adjusted to 7.5 for PAJ and LLA cultures and to 2 for GOR cultures. All procedures were conducted under sterile conditions in a laminar flow chamber (ESCO, Singapore) to prevent contamination. To enhance nutrient diffusion, the flasks were placed on an orbital shaker at 100 rpm inside a closed aerobic light chamber maintained at 24°C. The chamber was equipped with 10 LED lamps (18W, Unilux), providing a total light intensity of

>200 $\mu E \cdot m^{-2} \cdot s^{-1}$ under 12-hour light/dark cycles. Culture medium replenishment was performed every two weeks to maintain optimal growth of the bacterial communities.

Cyanobacteria and eukaryotic phototrophs were observed by optical microscopy and photosynthetic activity was assessed by fluorescence microscopy (CLSM FV1000, Olympus, Japan) weekly prior to experimentation, and after 14, 30, 60 and 90 days from the start of the expriment. Additionally, phototrophic cell biovolume was estimated by calculating the volume of individual cells using Infinity Analyze 7, Teledyne Lumenera (Teledyne Vision Solutions) and multiplying by cell count. Morphological identification was performed following Bergey's Manual of systematic bacteriology and Diaz & Maidana[53] for prokaryotes and diatoms, respectively. Identified morphotypes were corroborated against available literature from LLA[3][5], PAJ (Tebes-Cayo et al., 2019) and GOR[25]. Microorganisms, organic matrices and textures described in Cabestrero et al.[6] were used as a basis to describe the structures observed through microscopic techniques. Amoeba identification was based on Salazar et al.[54]. Imagery was obtained using Image Pro-Plus 6.0.0.260 with default settings.

2.3. Experimental Setting of Culture Experiments

After 3 months of incubation, a representative subsample of each salt flat was selected, their identifiers were LLA-115, PAJ-40 and GOR-48[6]. The selection was based on the cultures that exhibited the highest growth while maintaining a healthy green pigmentation. Each flask was subjected to bath sonication and homogenized by agitation. Then, 50 mL of each culture was extracted and placed inside previously autoclaved cylindrical glass containers with a sterile petri dish acting as lid that contained 150 mL of natural brine without BG-11 medium corresponding to each sampling site. Afterwards, 22 crystals from LLA, PAJ and GOR obtained as described in 2.1 were selected, with two from each morphology stored in Eppendorf tubes filled with paper as a control at t=0 for initial crystal texture descriptions. Then, 10 crystals of each morphology were placed inside the glass containers with inoculated brine, as well as corresponding abiotic controls consisting of autoclaved natural brine without inoculation. All glass containers were then placed inside the light chamber with the same configuration as described in 2.2. Water level was monitored and maintained through replenishment with distilled and autoclaved water to counter any effects of evaporation. Furthermore, cell counts, and optical/fluorescent microscopy were performed periodically to assess microbial growth with the same approach earlier described for the biomass generation process. Additionally, in response to unexpected acidophilic fungal contamination in GOR cultures, they were treated with a previously tested Sigma A5955 antibiotic-antimycotic.

2.4. Sample Preparation and SEM-EDS Analysis

To perform these analyses, one gypsum crystal was collected from each container (six in total) using plastic tools to avoid damaging the samples and then placed in plastic multi-well plates. Between each crystal collection, all tools and surfaces were sterilized with 80% ethanol to avoid cross-contamination of samples. To fix microbial cells present in the samples, 2 mL of 4% paraformaldehyde was added to each well left for 24 hours and removed afterwards. Then, to dehydrate the samples without causing cell collapse, 20-minute ethanol cycles were performed with 2 mL of 20%, 40%, 60%, 80%, 90%, 95%, 98% and 100% ethanol, the latter being performed overnight. Dilutions were made using the corresponding non-inoculated water of each sample. Ethanol was partially evaporated or extracted from the wells to proceed with the mounting of each crystal on aluminum specimen holders and carbon tape to fix the samples to the holder using sterilized plastic tools. Afterwards, samples were gold-coated using a Desk II Denton Vacuum LLC sputter coater (Moorestown, NJ, USA) to improve image quality during the SEM-EDS analysis. SEM imaging was performed using a Hitachi SU5000 (Hitachi, Tokyo, Japan) FE-SEM at 15 kV accelerating voltage, 11.8 mm working distance, and emission current of 145 µA in backscattered electron mode. This instrument was equipped with energy dispersive X-ray spectroscopy to obtain elemental composition of samples, along with spectral mapping. These analyses were repeated after 14, 30, 60 and 90 days to analyze textural changes in the gypsum crystals. Importantly, to maintain a rigorous distinction between biotic and abiotic systems, any film-like structures or embedding phases observed on the control crystals were classified strictly as amorphous abiotic precipitates rather than EPS, consistent with the confirmed absence of microbial growth in these samples.

2.5. X-Ray Diffraction

Powdered samples were analyzed to confirm SEM observations using X-ray diffraction (Cu-Kα, λ = 1.5406 Å) using a Bruker D8 Advance operated at 40 kV and 30 mA with a step size of 0.02° 2θ every 2 seconds. Diffraction patterns obtained from samples with high amorphous phase content were corrected using smoothing and baseline corrections through software. Semi-quantification was performed in Bruker DIFFRAC.EVA (version 12.0; Bruker AXS, 2005) coupled with the ICDD software using the PDF4+ 2021 database[55].

3. Results

In this section, we present the morphological and compositional data of gypsum crystals from Salar de Llamara (LLA), Salar de Pajonales (PAJ), and Salar de Gorbea (GOR) over the course of the incubation period. By comparing experimental and abiotic control samples over time, these data illustrate significant differences between microbe-modulated and abiotic dissolution of gypsum. Furthermore, we detail the development of extracellular polymeric substances (EPS) on crystal surfaces and the precipitation of mineral phases within the organic matrix, ultimately revealing specific microbe-mineral relationships that drive mineralogical transformations.

3.1. Brine Geochemistry and Gypsum Initial Conditions

For all selected brine samples, the gypsum saturation index (SI) indicated near equilibrium prior to forced precipitation through evaporation (Table 1), which was needed for crystal obtaining. For instance, LLA showed a SI value of 0, while PAJ showed -0.01, and GOR showed 0.14. Experimentally, gypsum precipitation was observed after the brines lost approximately 30% of their water volume through evaporation under the forced conditions described in Section 2.1.

Salt flat		Llamara	Pajonales	Gorbea
Date	**MM/DD/YY**	**9/14/2020**	**10/22/2019**	**3/12/2020**
Water parameter	Unit			
Na^+	mg/L	6330	41538	9970
Mg^{2+}	mg/L	130	2776	4110
Ca^{2+}	mg/L	780	7260	764
K^+	mg/L	176	1720	762
Mn^{2+}	mg/L	0	0	73
Cl^-	mg/L	7720	86240	21100
$SO4^{2-}$	mg/L	5680	1970	20550
Fe^{2+}	mg/L	0.3	0.8	66.6
Alkalinity	mg/L HCO_3^-	300	457	0
Salinity	%	2.9	15.2	6.0
EC	µS/cm	27140	169700	61300
Temperature	ºC	21.1	10.2	18.0
pH		8.3	7.4	1.9
Gypsum SI	log Q/K	0.00	-0.01	0.14
Glauberite SI	log Q/K	-2.95	-2.42	-2.19
Halite SI	log Q/K	-3.26	-1.29	-2.57
Thenardite SI	log Q/K	-3.40	-2.90	-2.77
Calcite SI	log Q/K	1.08	1.68	-

Table 1. Geochemistry of water samples used for culturing and experimentation without evaporation.

The gypsum crystals that grew from natural brine evaporation exhibited strikingly different initial

morphologies (Fig. 3). Crystals precipitated from LLA brine were mostly prismatic, slender forms reaching lengths of up to 3 mm (Fig. 3A). In contrast, those from PAJ were considerably larger (up to 3 cm) and displayed a well-developed tabular habit (Fig. 3B). These showed fishtail twinning and occasional overgrowths, expressed as delicate tabular crystals roughly 50 µm wide that adhered to the main surfaces. GOR samples, on the other hand, were composed of fine acicular crystals extending to about 4 mm in length (Fig. 3C). Under optical and scanning electron microscopy (Fig. 3A–F), all gypsum crystals appeared relatively smooth; yet closer inspection revealed subtle differences. GOR crystals exhibited more irregular surfaces, showing early signs of dissolution along their edges and sparse mineral aggregates on top (Fig. 3F). Together, these textural and morphological contrasts likely influenced the distinct evolutionary trends observed between the experimental runs and the abiotic controls described in the next sections.

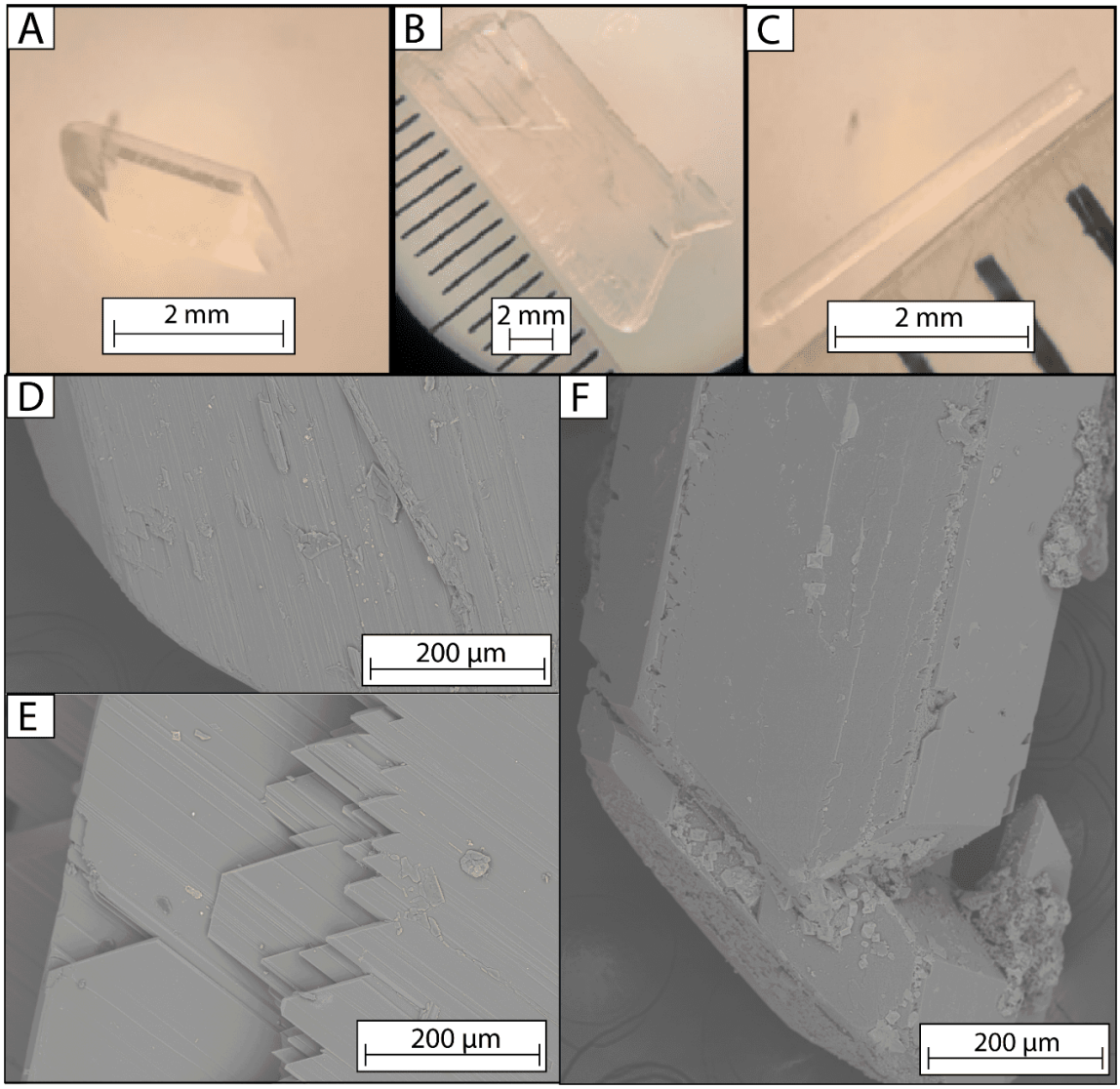


Figure 3. Gypsum crystal morphologies observed in each salt flat brine under binocular lenses (A-C) and microphotographs captured via SEM (D-F). (A) Prismatic LLA gypsum crystal without exposed cleavage planes and no apparent twinning. (B) Tabular PAJ gypsum crystal with exposed cleavage planes and characteristic fishtail twinning. (C) Acicular GOR gypsum crystal with characteristic elongated C axis. (D) Well-developed prismatic LLA crystal with no signs of dissolution. (E) Tabular PAJ crystal displaying cleavage planes, fishtail twinning and no dissolution. (F) Twinned acicular GOR crystal and occasional halite aggregates atop.

3.2. Resulting Conditions: Culture Development

Cultures exhibited significant changes in coloration, turbidity, and microbial abundance over the course of the experiment (Table 2). The following paragraphs detail these findings, integrating visual

observations, microbial dynamics, and mineral transformations.

Bacterial growth curves revealed similar trends between LLA and PAJ cultures, while GOR displayed a notably different pattern. In particular, LLA cultures were initially transparent with minimal turbidity, but they acquired green hue as they were dominated by photosynthetic microorganisms after a week. Moreover, LLA cultures experienced exponential growth of photosynthetic cells between days 14 and 60, while maintaining green coloration, after which a short plateau and subsequent decline in cell count were observed (Fig. 4A). Similarly, PAJ cultures started transparent but acquired slightly moss green hue by 14 days, along with increased turbidity until 60 days, later shifting to a pale orange at 90 days. This color change is consistent with the photosynthetic pigment degradation observed under microscope, as well as the increase in abundance of non-photosynthetic cells (Fig. 4B). In contrast, GOR cultures evolved differently from PAJ and LLA cultures due to the growth of acidophilic fungi, which resulted in moderate turbidity from the start of the experiment (sterile controls were not affected). These cultures acquired a pale green hue after antifungal treatment, accompanied by the recovery of coccoid cyanobacteria until the end of experiment, as suggested by the absence of a bacterial death phase over the 3-month experimental period (Fig. 4C).

Culture	Time [days]	Quantitative analysis					Qualitative analysis		
		Average Photosinthetic cells [cell/mL]	Average active photosinthetic cells [cell/mL]	Average non-fluorescent cells [cell/mL]	Living[41]	Average cell biovolume [µm3/mL]	Color	Turbidity	
LLA	0	6.20.E+05	6.20.E+05	ND	100%	3.97.E+08	Colorless	*	
	14	4.33.E+06	3.66.E+06	1.24.E+07	84%	9.73.E+09	Pale green	*	
	30	4.37.E+06	1.17.E+06	1.28.E+07	27%	1.82.E+10	Apple green	**	
	60	6.78.E+07	1.94.E+07	1.94.E+07	29%	9.35.E+09	Apple green	***	
	90	2.71.E+06	6.78.E+05	ND	25%	5.42.E+08	Apple green	**	
PAJ	0	7.31.E+06	6.56.E+06	ND	90%	3.95.E+08	Colorless	*	
	14	5.87.E+06	2.69.E+06	3.41.E+06	46%	1.63.E+09	Green	**	
	30	9.01.E+06	6.27.E+06	3.80.E+06	70%	4.50.E+09	Orange	**	
	60	2.42.E+07	2.11.E+07	6.41.E+07	87%	4.51.E+09	Brown	***	
	90	2.42.E+05	ND	5.08.E+06	NM	1.01.E+09	Pale orange	**	
GOR	0	1.00.E+07	1.00.E+07	ND	100%	2.02.E+09	White	**	
	14	4.00.E+05	4.00.E+05	ND	100%	3.48.E+08	Light green	***	
	30	3.00.E+06	7.00.E+05	ND	23%	2.96.E+08	Moss green	**	
	60	2.15.E+07	1.04.E+07	ND	42%	3.57.E+08	Moss green	**	

Culture	Time [days]	Quantitative analysis					Qualitative analysis		
		Average Photosinthetic cells [cell/mL]	Average active photosinthetic cells [cell/mL]	Average non-fluorescent cells [cell/mL]	Living[41]	Average cell biovolume [µm3/mL]	Color	Turbidity	
	90	4.00.E+07	2.00.E+07	ND	50%	3.97.E+08	Pale green	**	

Table 2. Summary of development of cultures over time. Turbidity is indicated as * (low), ** (medium) and *** (high). ND: Not detected.

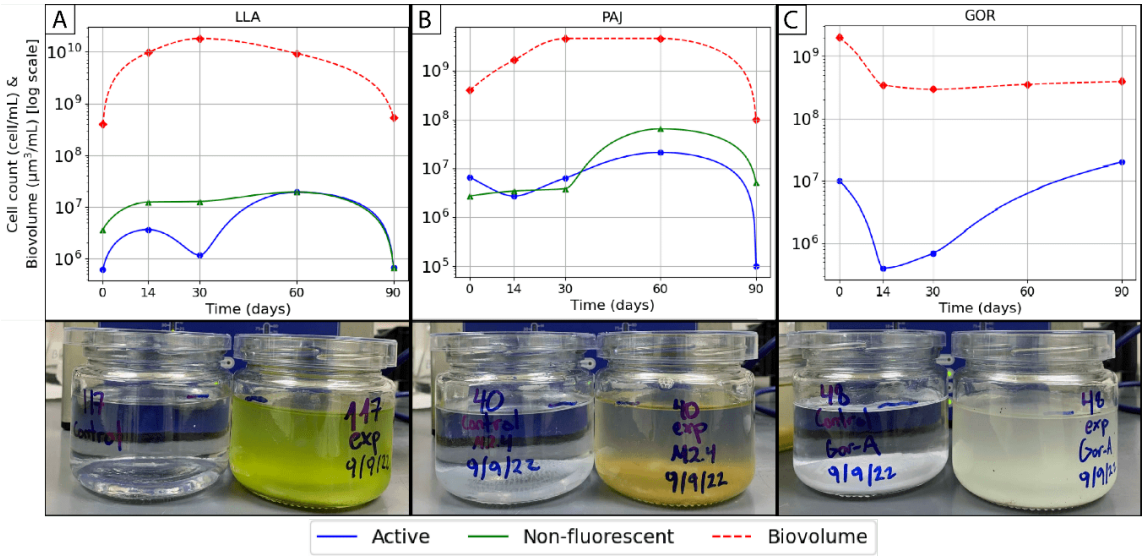


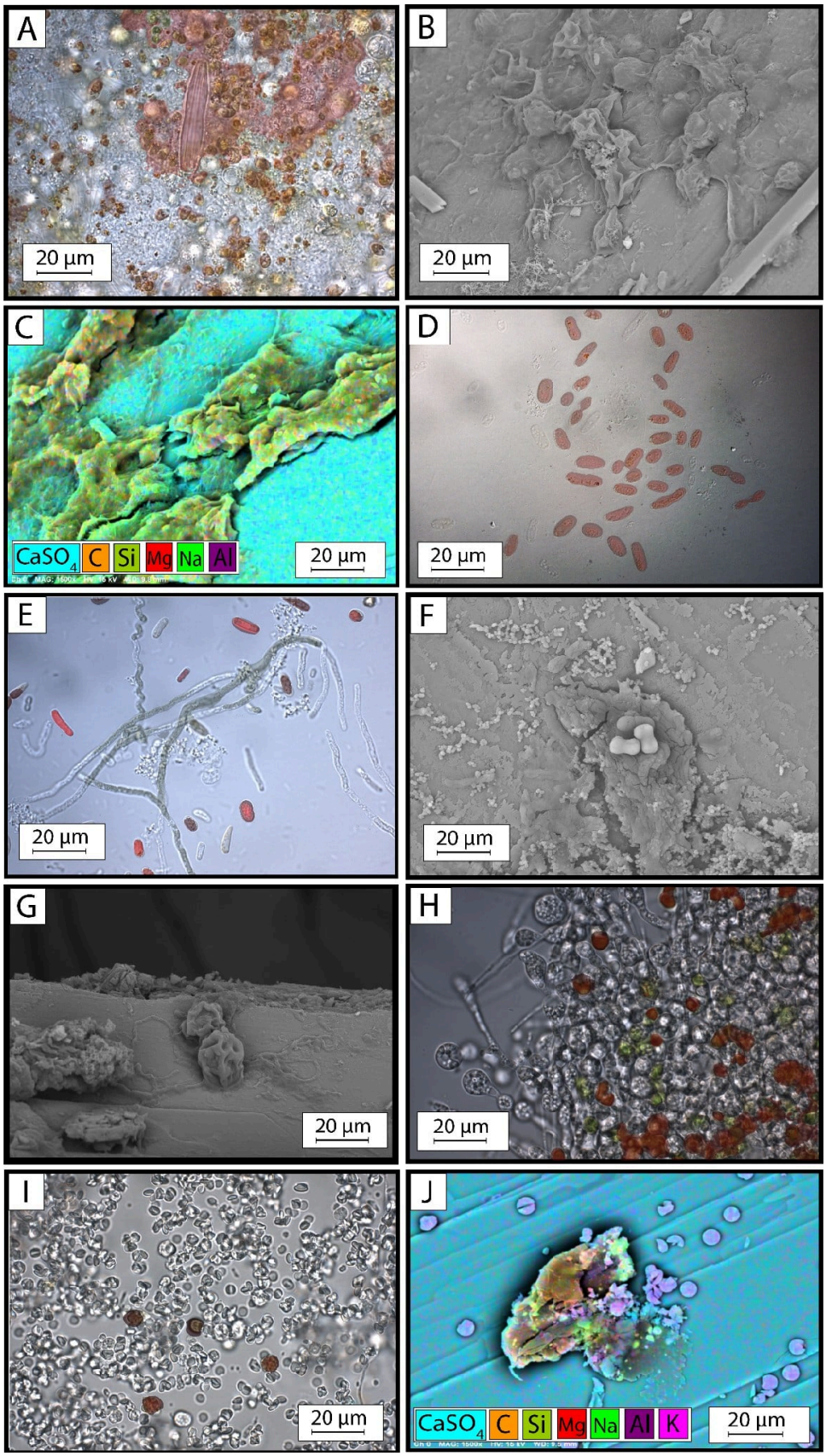
Figure 4. Experimental setup for gypsum dissolution under microbial growth in BG-11 medium with sterile brines, incubated at 24°C with constant agitation of 100 rpm in a closed aerobic light chamber, with a total light intensity of >200 $\mu E \cdot m^{-2} \cdot s^{-1}$ in 12-hour light/dark cycles. Specific growth curve for LLA (A), PAJ (B), and GOR (C) cultures. Below each graph, pictures of the containers after 90 days of experimentation (right side) and their corresponding control (left side) are shown. Note that control samples remained colorless and did not show microbial presence after 90 days.

doi.org/10.32388/ED4EYH.3

On the other hand, while all cultures exhibited microbial growth, each culture showed distinct predominant cellular morphotypes under the optical microscope. In each case, different relationships between microorganisms and crystals were also observed under SEM. For instance, cultures from Salar de Llamara were dominated by ~10 µm biflagellated oval algae resembling Dunalliella, and fusiform diatoms up to 50 µm compatible with Navicula (Fig. 5A), the latter being unique to LLA and becoming less prevalent by the end of experimentation. Furthermore, SEM observations showed that bacterial growth in LLA was followed by the embedding of small crystals and cells in a growing EPS matrix (Fig. 5B). By the end of the experiment, the EPS layer had thickened and covered most of the gypsum surface (Fig. 5C), which is consistent with the agglutination observed under optical microscopy. Additionally, EPS-embedded coccoid cells were attached to the gypsum crystal surface.

Conversely, PAJ cultures were dominated by bacillar cells resembling Dactylococcopsis in apparent active binary fission of up to 20 µm in size that exhibited red fluorescence (Fig. 5D). Additionally, and distinctively in PAJ, 150 µm spiral cyanobacteria similar to Spirulina were observed after 14 days of incubation, some of which had degraded pigments, along with Nodosilinea-like filamentous cyanobacteria (Fig. 5E). Like LLA, PAJ crystals were partially covered by EPS after the first 30 days of the experiment, and it embedded unicellular and diploid cells resembling of Gloeocapsa, newly formed sulfate crystals, and 5 µm dumbbell-shaped calcite on the gypsum (Fig. 5F). In addition, 10 µm globular organic structures were found adhered to the gypsum surface (Fig. 5G).

In parallel, conidia and conidiophores up to 60 µm long from unidentified acidophilic fungi overshadowed the scarce phototrophs in the GOR sample, which displayed fluorescence and a morphology compatible with the genus *Dunaliella* (Fig. 5H). After antifungal treatment, fungal presence declined and both algae and prokaryotes slowly recovered (Fig. 4C, 5I). Furthermore, and following the trend observed under optical microscopy, GOR crystals were covered by EPS at a slower pace after antimitotic treatment. By the end of the experiment, GOR crystals were partially covered in EPS-embedded photosynthetic coccoid cells and crystals, mainly those of lenticular morphology (Fig. 5J).



doi.org/10.32388/ED4EYH.3

Figure 5. Images of cell morphotypes and crystals observed in LLA, PAJ, and GOR cultures, combining bright field and epifluorescence microscopy (A, D, E, H, and I) with SEM-EDS micrographs (B, C, F, G, and J). (A) In LLA cultures, *Dunaliella*-like algae and Navicula-like fusiform diatoms are highlighted with red auto-fluorescence. (B–C) LLA crystals partially covered by a thick EPS layer embedding crystals and cells, also forming globular structures. (D) Bacillar diploids compatible with Dactylococcopsis with red auto-fluorescence in PAJ cultures. (E) Nodisilinea-like filaments and Spirulina-resembling spiral cyanobacteria resembling of showing degraded pigments in PAJ at 14 days of incubation. (F) PAJ tabular crystals covered globular aggregates within an EPS matrix with occasional dumbbell calcite. (G) Globular organic structures on PAJ gypsum crystal surface. (H) Conidia (yellow) and conidiophores (red) in the fungi-contaminated GOR outnumbering green algae (white) prior to antifungal treatment. (I) 2 to 5 µm lenticular crystals and 5 to 10 µm fluorescent algae in GOR after antimitotic treatment. (J) EPS embedded lenticular crystals and cells on top of the unaltered GOR crystals.

3.3. Gypsum Textural Evolution and Mineral Assemblages

Under experimental conditions, the interplay between gypsum dissolution and subsequent mineral precipitation varied depending on the presence or absence of microorganisms, as well as the initial microbial mat texture and gypsum crystal morphology inherent to each source salt flat sample (Fig. S2-S4).

In abiotic experiments, gypsum crystals showed textural alterations characterized by an apparent increase in porosity over time, as compared to inoculated samples. These pores had commonly jagged or abrupt edges throughout all samples, while their occurrence and morphology were distinct for each sample group. LLA crystals, for instance, started with a smooth surface but developed pronounced cleavage planes, along which dissolution occurred faster (Fig. 6A). As time progressed, fibrous eugsterite covered most of the crystal surface (Fig. 6B, Fig. S1). Later, the crystal surface became flaky with minerals filling the occasional elongated and circular pores. PAJ crystals, on the other hand, were smooth at the beginning, but quickly developed a flaky surface with increasing porosity of elongated, circular and irregular morphologies. These pores were not infilled with newly formed minerals, although occasional subhedral to euhedral halite and gypsum crystals were present in SEM and confirmed by XRD (Fig. 6C-D, Fig. S1). GOR crystals, by contrast, started with an already irregular surface that was partially covered by mineral aggregates identified as alunite (Fig. S1). As time progressed, occasional partially filled pores along planes and irregular fractures were observed (Fig. 6E-F) (Table 3).

	Time [day]	Gypsum surface	Porosity			Observed minerals
			Mean major axis size [µm]	Mean frequency [N/10000µm2]	Porosity filling	
LLA	0	Smooth	-	-	-	-
	14	Smooth	-	>2	No	Gypsum, fibrous eugsterite
	30	Porous, with dissolution along planes	20	>6	No	No change
	60	Fractures with dissolution along planes	50	>10	No	No change
	90	Fractures and dissolution along planes. Mineral cover	50	>10	Fibrous eugsterite	No change
PAJ	0	Smooth	-	-	-	-
	14	Porous/flaky	155	>6	No	Gypsum
	30	Porous/flaky	225	>9	No	Euhedral halite
	60	Porous/flaky	210	>10	No	No change
	90	Porous/flaky	335	>10	No	Mg-Si globules
GOR	0	Irregular edges and precipitates	-	-	-	-
	14	Irregular edges and precipitates	-	-	-	Gypsum, lenticular alunite
	30	Irregular edges and precipitates	-	-	No	No change
	60	Irregular edges and precipitates	-	-	Lenticular alunite	No change

doi.org/10.32388/ED4EYH.3

	Time [day]	Gypsum surface	Porosity			Observed minerals
			Mean major axis size [µm]	Mean frequency [N/10000µm2]	Porosity filling	
					aggregates	
	90	Irregular edges and precipitates	135	>4	Lenticular alunite aggregates	No change

Table 3.

doi.org/10.32388/ED4EYH.3

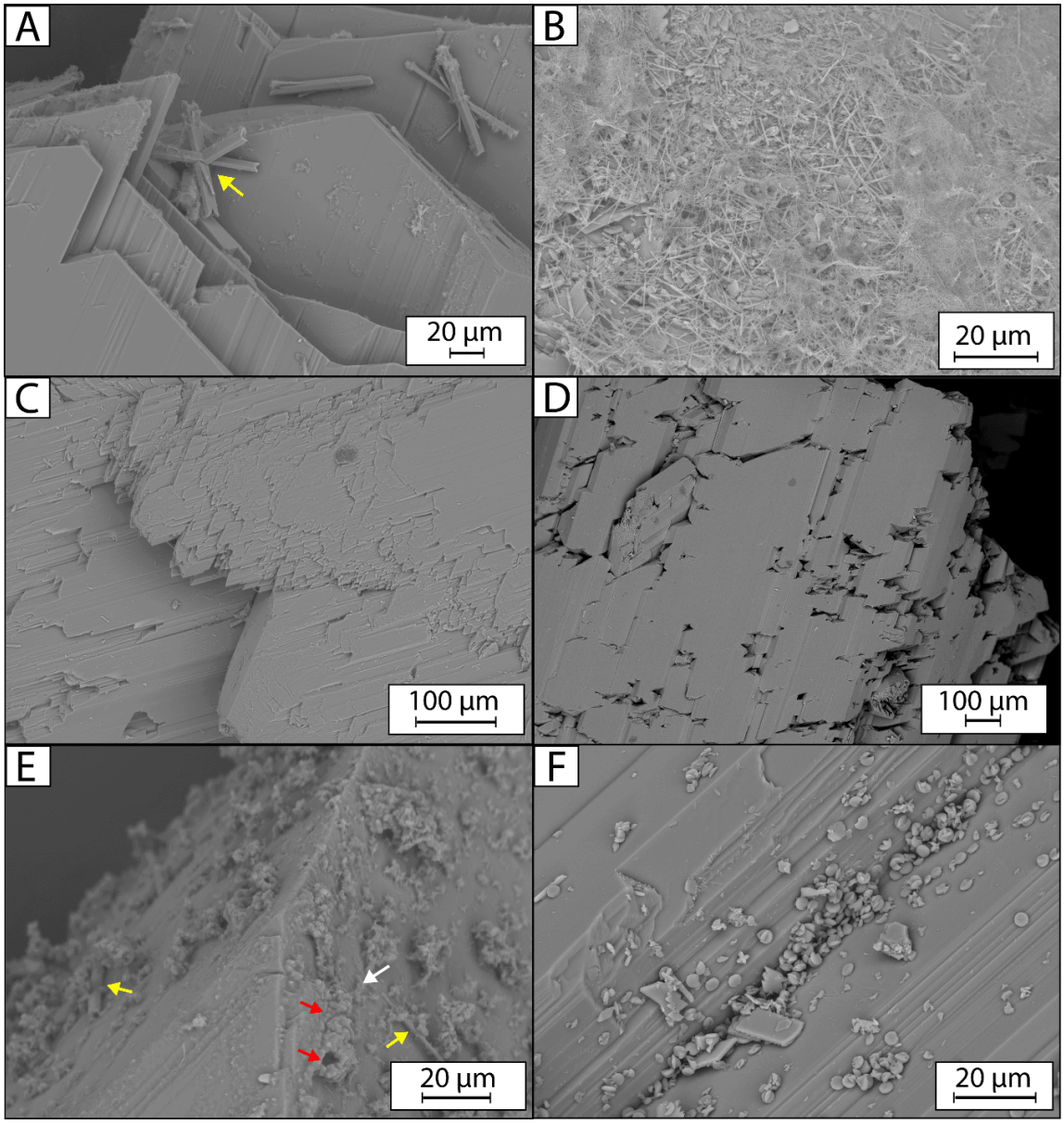


Figure 6. SEM microphotographs of LLA (A-B), PAJ (B-C) and GOR (E-F) control gypsum crystals. (A) Fishtail twinning, distinct cleavage planes and radial gypsum with fibrous aggregates atop (yellow arrow). (B) Fibrous eugsterite covering most of the gypsum surface. (C) Flaky and porous gypsum surface with exposed cleavage planes, and euhedral halite crystal. (D) Heavily dissolved gypsum surface, with several hundred micrometer fractures and cavities preferably along cleavage planes. (E) Newly formed gypsum (yellow arrows), fibrous eugsterite (white arrow) and scarce globular precipitates (red arrows) on top of the gypsum. (F) Twinned lenticular alunite crystals filling fractures in the gypsum, as well as newly formed prismatic gypsum.

doi.org/10.32388/ED4EYH.3

In the presence of microorganisms, by day 14, an EPS film had covered the surfaces of all crystal types, most prominently on LLA and PAJ crystals (Fig. 7). This biofilm progressively thickened while mineral precipitation occurred within its matrix at its surface. In LLA samples, prismatic eugsterie crystals (2–5 µm) formed preferentially associated with EPS as early as 14 days from the start of the experiment (Fig. 7A). These crystals increased in quantity throughout the experiment, becoming embedded in the EPS matrix, which by day 90 had contracted and formed globular and alveolar structures (Fig. 7B-C). In PAJ samples, on the other hand, dissolution features were present and filled from day 14, and became prominent by day 30, with halite and Mg-silicates forming preferentially on EPS within dissolution cavities (Fig. 7D). By day 60, isolated calcite crystals with dumbbell morphologies (3–6 µm) had appeared, as well as more Mg-silicates on the extending EPS layer (Fig. 7E). By the end of the experiment, apparent lenticular alunite crystals were also present (Fig. 7F). In GOR samples, new mineral formation was limited but included twinned lenticular aggregates of alunite with traces of organic material from day 14 onwards (Fig. 7G, Fig. S1), which increased in quantity towards day 60 (Fig. 7H). By the end of the experiment (day 90), GOR crystal surfaces were heavily altered, and the lenticular aggregates were apparently fully covered by EPS and newly formed gypsum (Fig. 7I) (Table 4).

When comparing dissolution and precipitation trends among abiotic and biotic cultures, notable differences and similarities emerge. For instance, LLA crystals in both cases showed limited abiotic dissolution, while eugsterite precipitation was notably faster in biotic experimental samples, as seen in early observations (Fig. 6A and 7A). In the case of PAJ samples, crystals without microbes displayed higher porosity and no filling, while experimental crystal porosities were filled by EPS and other minerals, notably dumbbell-shaped calcite (Fig. 6D and Fig. 7F). On the other hand, GOR crystals evolved similarly in both abiotic and biotic cultures, with gypsum dissolution apparently starting later than LLA and PAJ. The main difference between the samples was the apparent rate at which the lenticular aggregates accumulated on the gypsum surface, with biotic experimental samples displaying an apparently faster rate.

	Time [days]	Gypsum suface	Porosity			Newly observed minerals
			Mean major axis size [µm]	Mean frequency [N/10000µm2]	Porosity filling	
LLA	0	Smooth	-	-	-	-
	14	Alveolar organic cover	-	NM	EPS-embedded fibrous eugsterite crystals	Gypsum, fibrous Eugsterite
	30	Alveolar organic cover	20	>4	EPS-embedded 67 µm Gp crystals	No change
	60	Alveolar organic cover	50	>4	EPS-embedded Gp, eugsterite and Mg-Si globules	Mg-Si globules
	90	Alveolar organic/mineral cover	NM	>1	EPS-embedded Gp, eugsterite and Mg-Si globules	No change
PAJ	0	Smooth	-	-	-	-
	14	Smooth	NM	>1	Worm-like halite and 2 µm Mg-Si globules	Gypsum, allotriomorfic halite, Mg-Si globules
	30	Organic cover	115	>2	EPS-embedded 2 µm Mg-Si globules	Dumbbell-shaped calcite
	60	Organic cover	10	>1	Alveolar EPS-embedded 2 µm Mg-Si globules and Gp crystals	No change
	90	Organic cover	40	>1	Alveolar EPS-embedded 2 µm Mg-	Lenticular alunite

	Time [days]	Gypsum suface	Porosity			Newly observed minerals
			Mean major axis size [µm]	Mean frequency [N/10000µm2]	Porosity filling	
					Si globules and Gp crystals	
GOR	0	Irregular edges and precipitates	-	-	-	-
	14	Irregular edges and precipitates	-	-	-	Gypsum, lenticular alunite
	30	Irregular edges and precipitates	80	>6	Lenticular alunite aggregates	No change
	60	Organic/mineral cover	60	>2	Lenticular alunite aggregates and eugsterite	Fibrous eugsterite
	90	Organic/mineral cover	NM	>1	Lenticular alunite aggregates and eugsterite embedded in EPS	No change

Table 4. Summary of biotic experiment gypsum surface characteristics, porosity, and mineral precipitation over time (NM: not measured).

doi.org/10.32388/ED4EYH.3

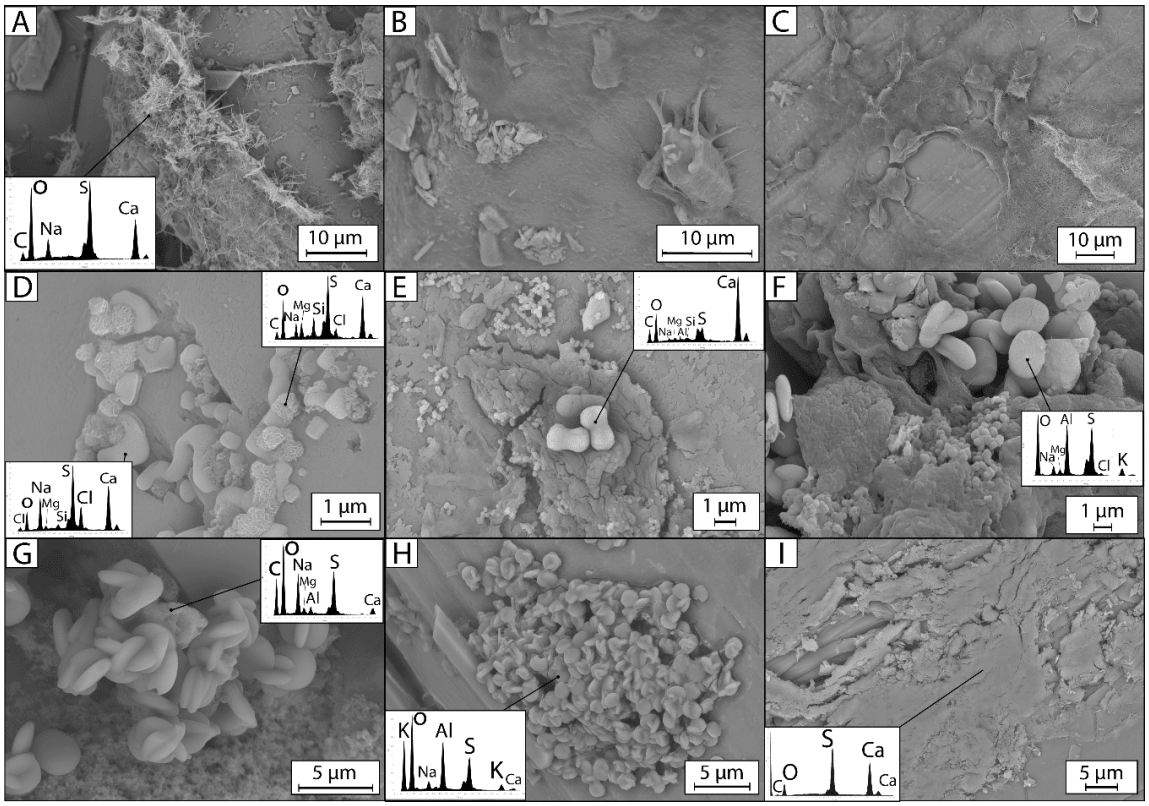


Figure 7. SEM microphotographs of LLA (A-C), PAJ (D-F) and GOR (G-I) gypsum crystals at 0 (first column), 35 (second column) and 90 days of experiments (third column). (A) Fibrous Na-Ca sulfate within and on top the alveolar EPS partially covering the LLA gypsum surface. (B) Thicker EPS layer embedding newly formed gypsum crystals. (C) Alveolar EPS embedding cells, fibrous Na-Ca sulfates and gypsum, and forming globular structures. (D) Mg-Silicate rugose globules and allotriomorphic halite filling porosities in PAJ gypsum. (E) Dumbbell-shaped calcite along with Mg-Si globules on the EPS. (F) Alveolar EPS-covered gypsum with Mg-Si globules and twinned lenticular K-Al sulfate on top. (G) Twinned lenticular K-Al sulfates with smooth surfaces with traces of C on a GOR gypsum crystal. (H) Lenticular crystal aggregates with jagged edges partially covering the gypsum surface, with scarce newly formed gypsum crystals. (I) Heavily altered gypsum surface with traces of carbon indicating organic matter.

4. Discussion

The experiments demonstrate that dissolution dynamics differ between biotic and abiotic systems, indicating that microbial activity actively modulates mineral alteration processes, as evidences by the textural changes observed in this study. Such influence affects dissolution patterns including their sizes, surface morphologies, and subsequent mineral formation, revealing that these processes are not

doi.org/10.32388/ED4EYH.3

exclusively controlled by abiotic factors. These results align with previous observations of microbially mediated gypsum alteration and replacement[6][56][57] (, among many others). Overall, the evidence presented here suggests that traditional abiotic models of brine and evaporite evolution should be revisited, emphasizing the need to integrate biochemical interactions into the framework governing the evolution of Andean and other salt flat deposits.

4.1. Microbial Community Dynamics

The experimental setup used BG11 medium to favor photosynthetic microorganisms and increase biomass prior to gypsum exposure. Although this enrichment reduced the original community complexity, a normal and well-documented phenomenon when reproducing microbial consortia in laboratory microcosms[58], the resulting cultures still retained the most abundant phototrophic groups characteristic of each salt flat (Figure 5)[3][59][25][8] (Tebes-Cayo et al., 2021). Furthermore, while natural brine samples were employed, highly variable environmental factors such as wind, solar radiation, and sediment dynamics were deliberately kept fixed for a controlled assessment of microbe-gypsum interactions. Despite these controlled laboratory conditions, each microbial consortium followed a distinct ecological trajectory likely influenced by its native community composition and site-specific geochemistry. Future studies could incorporate these fluctuating variables to simulate conditions even closer to the natural reality of Andean salt flats.

Specifically, in LLA and PAJ cultures, microbial growth followed a typical pattern, with photosynthetic cell abundance peaking after 60 days, accompanied by a progressive increase in both cell numbers and extracellular polymeric substances (EPS) attached to gypsum surfaces (Table 2, Figure 4). The microorganisms enriched from LLA were consistent with previous descriptions of this salt flat, where diatoms and Cyanobacteriota constitute major components of microbial mats[3][5]. Under the experimental conditions, LLA cultures contained a mixed assemblage heavily dominated by *Dunaliella*-like biflagellated algae and *Navicula*-like fusiform diatoms, alongside EPS-embedded coccoid cells (Figure 5A-C). This dominance likely enhanced primary production and promoted rapid development of EPS-rich microenvironments. By comparison, the PAJ consortium reflected the strong cyanobacterial signature reported for this site[23][8]. PAJ cultures were overwhelmingly dominated by cyanobacteria displaying a broad morphological diversity, including *Dactylococcopsis*-like bacillar cells in active binary fission, *Spirulina*-like and *Nodosilinea*-like filaments, and *Gloeocapsa*-like diploids (Figure 5D-G). This coexistence

of versatile morphotypes enabled extensive substrate colonization and EPS production, both of which are key processes in microbe-mineral interactions.

Despite these compositional contrasts, the responses of the LLA and PAJ consortia converged toward remarkably similar mineral-associated behaviors. In both cases, phototrophic growth promoted the accumulation of EPS, the colonization of surface irregularities, and the agglutination of newly formed mineral particles (Figures 5 and 7). Such convergence suggests that the capacity to modify the gypsum microenvironment is linked less to the presence of specific taxa than to shared functional traits widely distributed among phototrophic microorganisms, particularly cyanobacteria and associated microalgae. Cyanobacteria, for example, are among the most efficient EPS producers within photosynthetic mats, especially under environmental stress[60][61]. The localized activity of these specific phototrophs directly contributed to the extensive EPS coverage and mineral agglutination observed in our experiments.

Unlike the LLA and PAJ consortia, GOR cultures displayed a delayed response to enrichment and overall slower culture development, as revealed by SEM observations and cell counts (Figures 4 and 7). This initial lag most likely reflects a combination of the necessary antifungal treatment applied during culture preparation, which inadvertently stressed the populations, and the inherently slow growth rates typical of specialized extremophiles adapted to the extremely acidic conditions of Salar de Gorbea[24][22][62]. Nevertheless, after 60 days of incubation, the abundance of prokaryotes (Fig. 4C) and eukaryotes (Fig. 5H, 5I) in GOR increased noticeably. This eventual recovery demonstrates the resilience of these extremophilic communities. The predominance of *Dunaliella acidophila*-like acidophilic algae is particularly noteworthy, as that member of the *Dunaliella* genus is well known for their ability to thrive under low pH and saline conditions[63], indicating that the enrichment preserved key ecological features of the original ecosystem despite the imposed laboratory constraints.

Extensive microbial colonization of gypsum was also observed, particularly within round-edged cavities in the crystals (Fig. 7D-F). Cyanobacteria are well documented to actively bore into gypsum crystals to form these endolithic colonies[64][36][37]. Many authors have attributed this endolithic colonization pattern to the unique hydric properties of gypsum, which allow for humidity to be retained under hyperarid conditions[65][66][35]. For instance, the relative humidity within the gypsum crust at Salar de Pajonales fluctuates between 13% and 36%, reaching higher peaks during rare and brief rain events[8]. Similar microclimatic retention has also been reported at Llanos de la Paciencia[65], Lomas de Tilocar and Cordón de Lila[66][35], and in the southernmost part of the Tarapacá Region[33]. In our experiments,

endolithic colonization occurred despite the crystals being continuously submerged in a water column without evaporation, as water level was maintained throughout the experiment. This suggests that migrating into the mineral matrix may be a strategy of endolithic microorganisms in a preemptive manner, considering the fluctuating behavior of water availability and UV radiation. In Andean salt flats, ecosystems are subject to severe seasonal and interannual fluctuations, where seemingly permanent pools can periodically desiccate over decades and refill when conditions become favorable again. Therefore, even when water is abundant, these microorganisms may colonize gypsum porosities, possibly utilizing the mineral as a structural refuge to ensure long-term survival against the return of extreme desiccation and environmental stress[40][64][36][37]. However, this apparent preemptive migration into the mineral appears not to be a passive process; by actively occupying and modifying these microhabitats, endolithic communities drive significant textural and chemical transformations in the gypsum matrix.

4.2. Gypsum Dissolution: Transformations Driven by Endolithic Colonization

Both control and microbial-inoculated gypsum crystals showed early evidence of dissolution within the first month of exposure (Figs. 6C and 7D). These features included cavities, fractures, and irregular dissolution along crystal edges. However, clear differences were observed between treatments (Tables 3 and 4). Cavities in the microbially exposed crystals had smooth and rounded walls, whereas those in the controls were jagged and angular. Dissolution in the control samples likely occurred because the brine used in the experiments was nearly undersaturated with respect to gypsum. The morphology of the smooth cavities in inoculated samples resembles features previously attributed to endolithic colonization. Rothschild et al.[64] first described microbial boring in gypsum, which Sanz-Montero et al.[67] and Wierzchos et al.[36][37] later associated with endolithic activity capable of penetrating mineral substrates. This process was also suggested in the present study: as microbial colonization of gypsum progressed, so did the appearance of these rounded cavities, though microbes or metabolites were not always present (Figs. 6D and 7D for abiotic-biotic contrast). Moreover, pores with similar morphologies to those found in control samples were also present and occasionally inhabited by microbes. This, in turn, suggests that both abiotic and microbially-mediated dissolution were happening simultaneously in the inoculated samples.

While baseline gypsum dissolution in the incubation was thermodynamically driven by the near-zero saturation indices of the brines (Table 1), the presence of a microbial biofilm actively impeded this abiotic

process (Tables 3 and 4). The mechanism for this biotic buffering relies on the physical occlusion of the mineral surface; as EPS and mineral precipitates accumulated within the crystal pores over time, they effectively shielded the underlying gypsum (Figure 7). This supports the model proposed by Venturi et al. [56], wherein EPS coatings significantly reduce ion mobility across the mineral–water interface. In the LLA and PAJ systems, the temporal correlation between maximum EPS coverage and lowest porosity is consistent with biofilm development limiting gypsum dissolution (Tables 3 and 4). This mechanism coexisted with the above mentioned boring of the crystals by endolithic colonies, which suggests that microbes first bore into the crystals (or occupy pre-existing pores), and then cover them with EPS as a defense mechanism.

In LLA samples, pore abundance and size were similar between controls and experiments, though they displayed different morphologies, with abiotically produced pores being angular and jagged compared to their round-walled microbially produced counterparts. This, again, suggests that microbial activity may also promote dissolution under certain conditions, for example, through endolithic boring or metabolic processes that destabilize the crystal structure[36][37] (Wang et al., 2020). Gypsum crystals in abiotic controls followed a more linear trend, for instance, LLA and GOR controls remained relatively intact, while PAJ crystals in the controls developed larger and more numerous cavities compared to their inoculated counterparts. Comparing this trend with the observed patterns in biotic experiments highlights the role of microbial metabolism in modifying gypsum stability. On the other hand, as a result of microbial population decline and photosynthetic cell death (Table 2, Figure 4), late stage inoculated samples may have been partially dominated by heterotrophs as well as other non-phototrophic bacteria. For instance, sulfate-reducing bacteria can use sulfate from gypsum as an electron acceptor, leading to mineral dissolution, while As (V)-reducing bacteria, common in PAJ and GOR waters, can also promote gypsum instability[68]. In addition, degradation of the EPS matrix can locally increase pH and lower the gypsum saturation index, favoring its replacement by carbonates, as reported by Thompson and Ferris[46], Cody and Cody[69], and Vogel et al.[48] (2010).

Despite these potential dissolution mechanisms, the lower porosity in inoculated gypsum crystals suggests overall slower gypsum dissolution in the presence of microorganisms (Tables 3 and 4). This may reflect the relatively short duration of the experiment, which could have limited non-phototrophic metabolisms such as sulfate-reduction to take place, which would destabilize gypsum and is also often referred as responsible for carbonate mineralization, which was partially observed in this study (Figure 7E). Another possibility is that pores were present but covered by EPS and therefore less visible (Figures

7C,E, I), which implies that further analyses (specifically removing the eps layer to analyze the gypsum surface) beyond the timeframe of this experiment are needed.

Gypsum dissolution was also observed associated with halite precipitation, both in the preparation of synthetic crystals and in the experimental microcosms. Previous studies[70][71] showed that gypsum solubility increases with NaCl concentration, reaching a maximum near 3 M, which correlates to the 15% NaCl (~2.97 M) of the PAJ brine. The localized precipitation of halite on gypsum surfaces therefore likely enhanced gypsum dissolution, an effect most evident in PAJ samples (Figs. 6D and 7D).

4.3. Other Microbe-Mineral Interactions

Mineral assemblages have been reported to be different in biotic and abiotic settings, for instance, Thompson & Ferris[46] indicate that microbial activity drives chemical imbalances such as calcification or alkalinization that would not happen in absence of life. Therefore, microbial activity has been considered a key factor controlling the differences in mineral assemblages formed in abiotic and biotic environments, though this idea has not been extensively explored[6]. In general, mineral assemblages that nucleated in control samples were monotone and found only on the surface of the gypsum crystal (Table 3), whereas in the presence of microorganisms, a more diverse array of minerals (Table 4) with distinct textures nucleated preferably in EPS-filled porosities and EPS-coated gypsum surfaces (Figs. 7 and 8). Moreover, nucleation was not observed in the water itself, further supporting the idea that microbial activity drives these nucleation processes through localized saturation in the EPS (Table 1). This ion sequestration mechanism, along with the liberation of ions once the organic matter is degraded, was proposed by Braissant et al.[72] and del Buey et al.[73]. Overall, the observations made in this study confirm that microbial consortia actively mediate the localized precipitation of distinct authigenic phases, such as Mg-silicates, carbonates, and complex sulfate arrangements, by concentrating ions within the EPS matrix, consistent with previous studies[74][6][8].

Newly formed halite, calcite and eugsterite displayed textural and structural features indicative of biochemical influence on their formation (Figure 7)[31][69]. Some of them include fibrous and radial crystal habits, irregular crystal boundaries, and the presence of lattice defects[75]. In several cases, crystals exhibited distorted or dumbbell-shaped morphologies (calcite in Fig. 7E), consistent with nucleation on organic matrices. Other features included porous crystal interiors and composite aggregates, which contrast with the more euhedral and homogeneous morphologies observed in abiotic controls (Figure 6). Microbially influenced textures highlight the role of EPS in lowering nucleation

barriers and directing crystal growth along biologically mediated pathways. Similar characteristics have been reported for gypsum and other minerals affected by microbial activity, including distinctive crystal morphologies and the development of crystal defects[31][46][75][76].

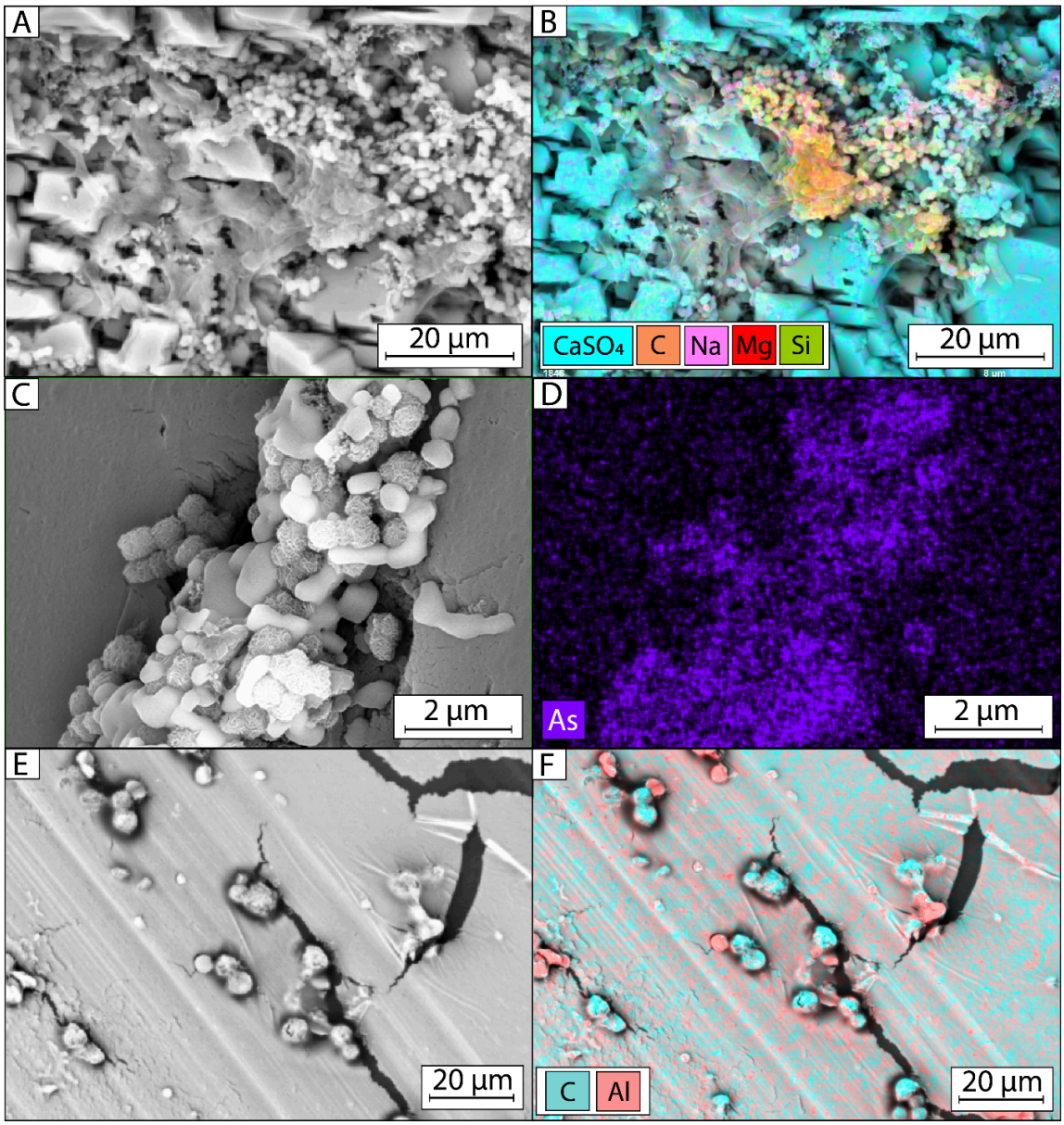


Figure 8. SEM microphotographs (A, C, E) and EDS mapping (B, D, F) of PAJ (A-B-C-D) and GOR (E-F) gypsum samples. (A) EPS-embedded crystals and Mg-Si globuleson heavily altered gypsum surface. (B) Mg-Si and Na are concentrated below the biomass, suggesting both Mg-Si globules and Na-Ca sulfates are agglutinated. (C) Porosity filled with allotriomorphic halite and Mg-Si globules. (D) Globules appear to be also As-rich according to EDS mapping. (E) Twinned lenticular aggregates covering GOR gypsum surface. (F) EDS mapping shows that they are rich in K, Al and S, suggesting alunite.

doi.org/10.32388/ED4EYH.3

The anionic functional groups within the EPS matrix appear to have promoted localized ion accumulation through the sequestration and late-stage liberation (through EPS degradation) of Na^{+}, Ca^{2+}, Mg^{2+}, K^{+}, and SO_4^{2-}[72][73]. This localized ion sequestration is directly supported by our EDS spectral mapping, which reveals a distinct concentration of these specific elements intrinsically associated with the carbon-rich biological matrices prior to macroscopic precipitation (Figs. 5C, 5J, and 8B). This microenvironmental supersaturation ultimately favored mineral nucleation. For instance, radial Na–Ca sulfates, likely corresponding to hydroglauberite ($Na_{10}Ca_3(SO_4)_8{\cdot}6H_2O$) or eugsterite, formed on and within the EPS matrix (Figs. 6A–B, 7A). On the other hand, during late stages of this experiment (Fig. 7C-F-I and Fig. 8B), the decline of organic matter cover on gypsum crystals, which is consistent with the biovolume analyses performed for the water column as well (Fig. 4), seems to be followed by mineral precipitation directly associated with the contracting EPS film. This dynamic aligns with the mechanisms described by Cabestrero et al.[10], where the activity of heterotrophic bacteria, which feed on EPS, favors the precipitation of carbonates and sulfates due to local alkalization along with the release of the ions previously captured within the organic matrix.

In PAJ, Mg–Si globules were detected exclusively in the presence of microorganisms. These globules, previously identified as protophyllosilicates by Cabestrero et al.[6], occurred within crystal porosities together with allotriomorphic halite (NaCl) embedded in EPS and organic material (Figs. 7D, 8C). The surrounding EPS was enriched in arsenic (Fig. 8D), suggesting selective ion binding within the matrix. Additionally, the dumbbell-shaped calcite ($CaCO_3$) crystals observed atop the EPS layer (Fig. 7E) likely correspond to those described by Lv et al.[77] as the result of prokaryote decay-driven biomineralization, along with the effect of negatively charged functional groups within the organic matrix.

Lenticular alunite (Fig. S1) aggregates appeared early in GOR (both control and experiment samples) and later in PAJ and LLA (Figs. 7F–G, 8E–F). Pueyo et al.[18] reported alunite as common in GOR, attributing its occurrence to hydrothermal input. The acidic pH of GOR brines and the high availability of Al ions may also favor alunite precipitation. Given that aluminum may be more concentrated in EPS than in the aqueous phase, its association with the biofilm could explain the preferential formation of alunite near microbial colonies. Although filtered brine was used, the early occurrence of alunite might also be related to mineral nucleation during the autoclaving process at 121 °C. Nevertheless, the spatial association between alunite crystals and coccoid cells along gypsum fractures in GOR (Fig. 5I) suggests a possible interaction between them. Regarding the possible alunite in late stage LLA and PAJ samples, it is possible that the release of aluminum ions as the organic matter decayed generated localized concentration of this

ion, which is comparatively less abundant in those brines than in GOR brines (2 to 5 ppm, [62]). This mechanism has been described for palygorskite and sepiolite by del Buey et al.[78], yet it has not been proposed specifically for alunite.

5. Conclusion

Our experiments demonstrate that microbial consortia from Andean salt flats actively alter gypsum dissolution pathways compared to purely abiotic microcosmos. Specifically, microbial colonization is strongly associated with the formation of characteristic rounded dissolution features and extensive extracellular polymeric substance (EPS) development. In contrast, abiotic dissolution under slightly subsaturated conditions preferentially generates angular cavities and fractures along crystal cleavage planes.

Furthermore, the progressive development of EPS-rich microenvironments significantly modifies gypsum surface evolution. This biological matrix appears to act as a physicochemical diffusion barrier that limits abiotic dissolution, while simultaneously serving as a preferential site for localized mineral nucleation. Consequently, authigenic mineral precipitation occurs predominantly within EPS-coated surfaces and cavities rather than in the surrounding bulk water column.

This biologically mediated mineral precipitation occurs even under non-evaporative conditions, producing distinct mineral assemblages that varied among microbial consortia and their corresponding brines. While fibrous eugsterite and Mg-silicates emerged as common products across different samples, site-specific assemblages also formed: cultures from Salar de Pajonales generated allotriomorphic halite and dumbbell-shaped calcite, whereas those from Salar de Gorbea exhibited lenticular alunite aggregates that became closely associated with the microbial EPS over time.

The specific mineral textures and mineral-organic associations generated in these experiments, such as alveolar-arranged eugsterite, Mg-Si globules, and dumbbell-shaped calcite, formed exclusively in the presence of microorganisms. Their consistent association with microbial colonization and EPS suggests that these unique formations may represent potential morphological biosignatures, offering valuable analogues for interpreting ancient terrestrial evaporitic systems and guiding astrobiological exploration in extraterrestrial targets.

Ultimately, these findings highlight that microbial activity substantially drives evaporite transformations. Therefore, biological processes should be explicitly integrated alongside

physicochemical controls into comprehensive conceptual models of salt-flat evolution. To further advance this integration, future studies should build upon these initial experiments by incorporating fluctuating environmental variables such as dynamic solar radiation and desiccation-recharge cycles, together with molecular and functional characterization of the microbial consortia, to better link microbial community composition and metabolic potential with mineral dissolution and precipitation processes under conditions representative of these polyextreme ecosystems.

Statements and Declarations

Funding

Proyecto CONICYT Postdoctorado 3190821, ANID National Doctoral Scholarship (No. 21181422) and Centro de Biotecnología “Profesor Alberto Ruiz” (CBAR-UCN). Additional support was provided to O.C. by MCIN/AEI/10.13039/5011000110033 under project PID2021-123735OB-C22/C21.

Author Contributions

C. T.-C., O. C. and C. D., designed and carried out the sampling campaigns at Salar de Llamara, Salar de Pajonales and Salar de Gorbea. O. C., C. T.-C. and I.D. O-V. designed the experimental setup with supervision of C. D., and I.D. O-V. executed the experiment under supervision from O.C. and C. T-C. CLSM and fluorescence imaging was carried out by I.D. O-V. and C. T.- C., and processed by I.D. O-V. Hidrogeochemical modelling and gypsum crystal obtention was performed by I.D. O-V. with supervision of O. C. Sampling for SEM-EDS analyses was performed by I.D. O-V., and sample preparation was carried out by I.D. O-V. and O. C. SEM-EDS analyses were performed at MAINI under supervision from O. C., C. T.-C. and I.D. O-V. Sampling, processing and interpretation of XRD analyses were performed by B.M under supervision from O.C. Data discussion was coordinated by I.D. O-V. with aid from O. C, C. T-C. and C.D. Manuscript was written by I.D. O-V., with contributions from all authors.

Data Availability

The data that support the findings of this study (including SEM-EDS micrographs, XRD diffractograms, cell counts, biovolume calculations, and hydrogeochemical parameters) are available from the corresponding author (I.D. Orellana-Villota) upon reasonable request.

Acknowledgments

The authors are appreciative of the support from the staff at MAINI® for facilitating access to the XRD (FONDEQUIP EQM230017) and SEM (FE-SEM SU5000-MAINI® UCN 2018) equipment. The authors also thank CBAR and its personnel (Universidad Católica del Norte, Antofagasta, Chile) for facilitating access to their laboratory facilities.

References

1. a, b *Warren JK (2006). Evaporites: Sediments, Resources and Hydrocarbons. Berlin: Springer.*
2. a, b *Chong Díaz G, Demergasso C, Urrutia Meza J, Vargas M (2020). "El Dominio Salino del Norte de Chile y S us Yacimientos de Minerales Industriales" [The Saline Domain of Northern Chile and Its Industrial Mineral Deposits]. Boletín de la Sociedad Geológica Mexicana [Bulletin of the Mexican Geological Society]. **72**:e1805 20.*
3. a, b, c, d, e, f, g *Demergasso C, Chong G, Galleguillos P, Escudero L, Martínez-Alonso M, Esteve I (2003). "Tapet es Microbiales del Salar de Llamará, Norte de Chile" [Microbial Mats of the Salar de Llamara, Northern Chil e]. Revista Chilena de Historia Natural [Chilean Journal of Natural History]. **76**:485–499.*
4. ^ *Lee CJD, McMullan PE, O'Kane CJ, Stevenson A, Santos IC, Roy C, Ghosh W, Mancinelli RL, Mormile MR, Mc Mullan G, Banciu HL, Fares MA, Benison KC, Oren A, Dyall-Smith ML, Hallsworth JE (2018). "NaCl-Saturate d Brines Are Thermodynamically Moderate, Rather than Extreme, Microbial Habitats." FEMS Microbiol Re v. **42**:672–693.*
5. a, b, c, d, e, f, g, h *Reid RP, Oehlert AM, Suosaari EP, Demergasso C, Chong G, Escudero LV, Palma AT (2021). "El ectrical Conductivity as a Driver of Biological and Geological Spatial Heterogeneity in the Puquios, Salar de Llamara, Atacama Desert, Chile." Sci Rep. **11**:12769.*
6. a, b, c, d, e, f, g, h, i, j, k, l, m, n *Cabestrero Ó, Tebes-Cayo C, Hinman NW, Demergasso C (2022). "Mineral Parage nesis Precipitating in Salt Flat Pools of Continental Environments Replicated in Microbial Mat Microcosms Without Evaporation." Minerals. **12**:646.*
7. ^ *Wierzchos J, Ascaso C, McKay CP (2006). "Endolithic Cyanobacteria in Halite Rocks from the Hyperarid Co re of the Atacama Desert." Astrobiology. **6**:415–422.*
8. a, b, c, d, e, f, g, h, i *Tebes-Cayo C, Demergasso C, Cabestrero Ó, Chong G, Carrizo D, Sánchez-García L, Parro V, Warren-Rhodes K, Cabrol N, Echeverría-Vega A, Castro-Nallar E, Menzies A, Sanz-Montero ME (2026). "Gyp*

*sum as a Repository of Extinct and Extant Biosignatures at Salar de Pajonales, Northern Chile." Front Astro n Space Sci. **12**:1693302.*

9. ^a, ^b*Cabestrero Ó, Sanz-Montero ME (2016). "Microbially Mediated Sulfate Precipitation in Ephemeral Saline Lakes of Central Spain: Implications for Brine Evolution and Evaporite Formation." J Paleolimnol. **55**:123–13 9.*
10. ^a, ^b*Cabestrero Ó, Sanz-Montero ME, Arregui L, Serrano S, Visscher PT (2018a). "Seasonal Variability of Mine ral Formation in Microbial Mats Subjected to Drying and Wetting Cycles in Alkaline and Hypersaline Sedim entary Environments." Aquat Geochem. **24**:79–105.*
11. ^*Jahnke LL, Des Marais DJ (2019). "Carbon Isotopic Composition of Lipid Biomarkers from an Endoevaporit ic Gypsum Crust Microbial Mat Reveals Cycling of Mineralized Organic Carbon." Geobiology. **17**:643–659.*
12. ^*Eugster HP, Hardie LA (1978). "Saline Lakes." In: Lerman A, ed. Lakes: Chemistry, Geology, Physics. New Yo rk, NY: Springer. pp. 237–293.*
13. ^*Lowenstein TK, Hardie LA (1985). "Criteria for Recognition of Salt-Pan Evaporites." Sedimentology. **32**:627 –644.*
14. ^*Warren JK (2016). Evaporites: A Geological Compendium. 2nd ed. Berlin: Springer.*
15. ^a, ^b*Boschetti T, Cortecci G, Barbieri M, Mussi M (2007). "New and Past Geochemical Data on Fresh to Brine Waters of the Salar de Atacama and Andean Altiplano, Northern Chile." Geofluids. **7**:33–50.*
16. ^a, ^b*Ortiz C, Risacher F, Chong G (2014). "Hydrogeochemical Evolution of Northern Chilean Salars." Hydrol Pr ocess. **28**:462–477.*
17. ^a, ^b*Risacher F, Alonso H, Salazar Méndez C (1999). "Geoquímica de Aguas en Cuencas Cerradas: I, II, III Regi ones-Chile" [Water Geochemistry in Closed Basins: I, II, III Regions-Chile]. Dirección General de Aguas.*
18. ^a, ^b, ^c*Pueyo Mur JJ, Demergasso C, Escudero L, Chong G, Corttéz-Rivera P, Sanjurjo-Sánchez J, Giralt Romeu S (2021). "On the Origin of Saline Compounds in Acidic Salt Flats (Central Andean Altiplano)." Chem Geol. **5 74**:120155.*
19. ^a, ^b*Farías ME, Contreras M, Rasuk MC, Kurth D, Flores MR, Poiré DG, Visscher PT (2014). "Characterization o f Bacterial Diversity Associated with Microbial Mats, Gypsum Evaporites and Carbonate Microbialites in Th alassic Wetlands: Tebenquiche and La Brava, Salar de Atacama, Chile." Extremophiles. **18**:311–329.*
20. ^*Risacher F, Alonso H, Salazar C (2003). "The Origin of Brines and Salts in Chilean Salars: A Hydrochemical Review." Earth-Sci Rev. **63**:249–293.*
21. ^a, ^b*Rodríguez-Albornoz C (2018). "Geología de Salar de Pajonales (7.209.000-7.226.500 N.-510.000-530.000 E) y Antecedentes de Su Microbiota, Antofagasta, Norte de Chile" [Geology of Salar de Pajonales (7.209.000*

-7.226.500 N.-510.000-530.000 E) and Background of Its Microbiota, Antofagasta, Northern Chile]. Universi dad Católica del Norte.

22. a, b, c *Escudero LV, Bijman J, Chong G, Demergasso C (2013). "Geochemistry and Microbiology in an Acidic, Hi gh Altitude (4,000 m) Salt Flat—High Andes, Northern Chile." Adv Mater Res. **825**:28–32.*
23. a, b *Warren-Rhodes K, Cabrol NA, Phillips M, Tebes-Cayo C, Kalaitzis F, Ayma D, SETI Institute NAI Team (20 23). "Orbit-to-Ground Framework to Decode and Predict Biosignature Patterns in Terrestrial Analogues." N at Astron. **7**:406–422.*
24. a, b, c *Davis-Belmar CS, Pinto E, Demergasso C, Rautenbach G (2013). "Proteo and Actinobacteria Diversity at a Sulfide, Salt and Acid-Rich Lake in the North of Chile." Adv Mater Res. **825**:37–41.*
25. a, b, c *Escudero L, Oetiker N, Gallardo K, Tebes-Cayo C, Guajardo M, Nuñez C, Demergasso C (2018). "A Thiotr ophic Microbial Community in an Acidic Brine Lake in Northern Chile." Antonie Van Leeuwenhoek. **111**:140 3–1419.*
26. ^ *Demergasso CS, Guillermo CD, Lorena EG, Mur JJP, Pedrós-Alió C (2007). "Microbial Precipitation of Arseni c Sulfides in Andean Salt Flats." Geomicrobiol J. **24**:111–123.*
27. ^ *Dupraz C, Reid RP, Braissant O, Decho AW, Norman RS, Visscher PT (2009). "Processes of Carbonate Precipi tation in Modern Microbial Mats." Earth-Sci Rev. **96**:141–162.*
28. ^ *Rickard D (2012). Sulfidic Sediments and Sedimentary Rocks. Amsterdam: Elsevier.*
29. ^ *Chen S, Watkins JM (2025). "Oxygen and Carbon Isotopes in Marine Carbonates: A Biogenic Climate Archi ve Built Upon Disequilibria." Elements. **21**:112–117.*
30. ^ *Daëron M, Drysdale RN, Peral M, Huyghe D, Blamart D, Coplen TB, Zanchetta G (2019). "Most Earth-Surfac e Calcites Precipitate Out of Isotopic Equilibrium." Nat Commun. **10**:429.*
31. a, b, c *Cody RD, Cody AM (1988). "Gypsum Nucleation and Crystal Morphology in Analog Saline Terrestrial E nvironments." J Sediment Res. **58**:247–255.*
32. ^ *Nicoleau L, Van Driessche AE, Kellermeier M (2019). "A Kinetic Analysis of the Role of Polymers in Mineral Nucleation. The Example of Gypsum." Cem Concr Res. **124**:105837.*
33. a, b *Cámara B, Souza-Egipsy V, Ascaso C, Artieda O, De Los Ríos A, Wierzchos J (2016). "Biosignatures and Mi crobial Fossils in Endolithic Microbial Communities Colonizing Ca-Sulfate Crusts in the Atacama Desert." C hem Geol. **443**:22–31.*
34. ^ *Meslier V, Casero MC, Dailey M, Wierzchos J, Ascaso C, Artieda O, DiRuggiero J (2018). "Fundamental Driver s for Endolithic Microbial Community Assemblies in the Hyperarid Atacama Desert." Environ Microbiol. **20**: 1765–1781.*

35. ^a ^b ^cWierzchos J, DiRuggiero J, Vítek P, Artieda O, Souza-Egipsy V, Škaloud P, Ascaso C (2015). "Adaptation Strategies of Endolithic Chlorophototrophs to Survive the Hyperarid and Extreme Solar Radiation Environment of the Atacama Desert." Front Microbiol. **6**:934.

36. ^a ^b ^c ^d ^eWierzchos J, Casero MC, Artieda O, Ascaso C (2018). "Endolithic Microbial Habitats as Refuges for Life in Polyextreme Environment of the Atacama Desert." Curr Opin Microbiol. **43**:124–131.

37. ^a ^b ^c ^d ^e ^fWierzchos J, Ascaso C, Artieda O, Casero MC (2020). "The Desert Polyextreme Environment and Endolithic Habitats." In: Farías ME, ed. Microbial Ecosystems in Central Andes Extreme Environments: Biofilms, Microbial Mats, Microbialites and Endoevaporites. Cham: Springer. pp. 37–49.

38. ^Benison KC, Karmanocky FJ III (2014). "Could Microorganisms Be Preserved in Mars Gypsum? Insights from Terrestrial Examples." Geology. **42**:615–618.

39. ^Huang W, Ertekin E, Wang T, Cruz L, Dailey M, DiRuggiero J, Kisailus D (2020). "Mechanism of Water Extraction from Gypsum Rock by Desert Colonizing Microorganisms." Proc Natl Acad Sci U S A. **117**:10681–10687.

40. ^a ^bFriedmann EI (1980). "Endolithic Microbial Life in Hot and Cold Deserts." Orig Life. **10**:223–235.

41. ^a ^bRoldán M, Ascaso C, Wierzchos J (2014). "Fluorescent Fingerprints of Endolithic Phototrophic Cyanobacteria Living Within Halite Rocks in the Atacama Desert." Appl Environ Microbiol. **80**:2998–3006.

42. ^Friedmann EI, Kibler AP (1980). "Nitrogen Economy of Endolithic Microbial Communities in Hot and Cold Deserts." Microb Ecol. **6**:95–108.

43. ^Sajjad W, Ilahi N, Kang S, Bahadur A, Zada S, Iqbal A (2022). "Endolithic Microbes of Rocks, Their Community, Function and Survival Strategies." Int Biodeterior Biodegrad. **169**:105387.

44. ^Hinman NW, Hofmann MH, Warren-Rhodes K, Phillips MS, Noffke N, Cabrol NA, Parro V (2022). "Surface Morphologies in a Mars-Analog Ca-Sulfate Salar, High Andes, Northern Chile." Front Astron Space Sci. **8**:797591.

45. ^Harouaka K, Mansor M, Macalady JL, Fantle MS (2016). "Calcium Isotopic Fractionation in Microbially Mediated Gypsum Precipitates." Geochim Cosmochim Acta. **184**:114–131.

46. ^a ^b ^c ^dThompson JB, Ferris FG (1990). "Cyanobacterial Precipitation of Gypsum, Calcite, and Magnesite from Natural Alkaline Lake Water." Geology. **18**:995–998.

47. ^Jarwar MA, Dumontet S, Pasquale V, Chen C (2022). "Microbial Induced Carbonate Precipitation: Environments, Applications, and Mechanisms." Geomicrobiol J. **39**:833–851.

48. ^a ^bVogel MB, Des Marais DJ, Turk KA, Parenteau MN, Jahnke LL, Kubo MD (2009). "The Role of Biofilms in the Sedimentology of Actively Forming Gypsum Deposits at Guerrero Negro, Mexico." Astrobiology. **9**:875–893.

49. ^Kemper WD, Olsen J, De Mooy CJ (1975). "Dissolution Rate of Gypsum in Flowing Water." Soil Sci Soc Am J. **39**:458–463.

50. ^Liu ST, Nancollas GH (1973). "The Crystal Growth of Calcium Sulfate Dihydrate in the Presence of Additive s." J Colloid Interface Sci. **44**:422–429.

51. ^Witkamp GJ, Van der Eerden JP, Van Rosmalen GM (1990). "Growth of Gypsum: I. Kinetics." J Cryst Growth. **102**:281–289.

52. ^Parkhurst DL, Appelo CAJ (2013). "Description of Input and Examples for PHREEQC Version 3—A Compute r Program for Speciation, Batch-Reaction, One-Dimensional Transport, and Inverse Geochemical Calculatio ns." U.S. Geological Survey.

53. ^Díaz C, Maidana N (2005). Diatomeas de los Salares Atacama y Punta Negra, II Región, Chile [Diatoms of t he Atacama and Punta Negra Salt Flats, II Region, Chile]. Santiago, Chile: Centro de Ecología Aplicada Ltda.

54. ^Salazar-Ardiles C, Asserella-Rebollo L, Andrade DC (2022). "Free-Living Amoebas in Extreme Environmen ts: The True Survival in Our Planet." BioMed Res Int. **2022**:2359883.

55. ^Muñoz B (2023). "Simulación de la Precipitación Mineral de Salares del Norte de Chile Obtenida Tras Evap orar Salmueras en Presencia y Ausencia de Microorganismos" [Simulation of Mineral Precipitation in Salt F lats of Northern Chile Obtained After Evaporating Brines in the Presence and Absence of Microorganisms]. Universidad Católica del Norte.

56. a, bVenturi S, Crognale S, Di Benedetto F, Montegrossi G, Casentini B, Amalfitano S, Fazi S (2022). "Interplay Between Abiotic and Microbial Biofilm-Mediated Processes for Travertine Formation: Insights from a Ther mal Spring (Piscine Carletti, Viterbo, Italy)." Geobiology. **20**:837–856.

57. ^Jehlička J, Oren A, Vítek P, Wierzchos J (2024). "Microbial Colonization of Gypsum: From the Fossil Record t o the Present Day." Front Microbiol. **15**:1397437.

58. ^Osman JR, Wang Y, Jaubert C, Nguyen TN, Fernandes GR, DuBow MS (2021). "The Bacterial Communities o f Surface Soils from Desert Sites in the Eastern Utah (USA) Portion of the Colorado Plateau." Microbiol Res. **244**:126664.

59. ^Rasuk MC, Kurth D, Flores MR, Contreras M, Novoa F, Poiré DG, Farías ME (2014). "Microbial Characterizat ion of Microbial Ecosystems Associated to Evaporites Domes of Gypsum in Salar de Llamara in Atacama De sert." Microb Ecol. **68**:483–494.

60. ^Rossi F, De Philippis R (2015). "Role of Cyanobacterial Exopolysaccharides in Phototrophic Biofilms and in Complex Microbial Mats." Life. **5**:1218–1238.

61. ^Laroche C (2022). "Exopolysaccharides from Microalgae and Cyanobacteria: Diversity of Strains, Production Strategies, and Applications." Mar Drugs. **20**:336.

62. a, bTebes-Cayo C (2025). "El Rol de Los Microorganismos en el Origen y Evolución del Yeso Biogénico en Depósitos Salinos del Norte de Chile" [The Role of Microorganisms in the Origin and Evolution of Biogenic Gypsum in Saline Deposits of Northern Chile]. Universidad Católica del Norte.

63. ^Pick U (1999). "Dunaliella Acidophila—A Most Extreme Acidophilic Alga." In: Seckbach J, ed. Enigmatic Microorganisms and Life in Extreme Environments. Dordrecht: Springer. pp. 465–478.

64. a, b, cRothschild LJ, Giver LJ, White MR, Mancinelli RL (1994). "Metabolic Activity of Microorganisms in Evaporites 1." J Phycol. **30**:431–438.

65. a, bDong H, Rech JA, Jiang H, Sun H, Buck BJ (2007). "Endolithic Cyanobacteria in Soil Gypsum: Occurrences in Atacama (Chile), Mojave (United States), and Al-Jafr Basin (Jordan) Deserts." J Geophys Res Biogeosci. **112**:G02030.

66. a, bDiRuggiero J, Wierzchos J, Robinson CK, Souterre T, Ravel J, Artieda O, Ascaso C (2013). "Microbial Colonisation of Chasmoendolithic Habitats in the Hyper-Arid Zone of the Atacama Desert." Biogeosciences. **10**:2439–2450.

67. ^Sanz-Montero ME, Rodríguez-Aranda JP, Calvo JP (2006). "Mediation of Endoevaporitic Microbial Communities in Early Replacement of Gypsum by Dolomite: A Case Study from Miocene Lake Deposits of the Madrid Basin, Spain." J Sediment Res. **76**:1257–1266.

68. ^Rios-Valenciana EE, Briones-Gallardo R, Chazaro-Ruiz LF, Lopez-Lozano NE, Sierra-Alvarez R, Celis LB (2020). "Dissolution and Final Fate of Arsenic Associated with Gypsum, Calcite, and Ferrihydrite: Influence of Microbial Reduction of As (V), Sulfate, and Fe (III)." Chemosphere. **239**:124823.

69. a, bCody AM, Cody RD (1991). "Chiral Habit Modifications of Gypsum from Epitaxial-Like Adsorption of Stereospecific Growth Inhibitors." J Cryst Growth. **113**:508–519.

70. ^Ostroff AG, Metler AV (1966). "Solubility of Calcium Sulfate Dihydrate in the System NaCl-MgCl2-H2O from 28° to 70° C." J Chem Eng Data. **11**:346–350.

71. ^Reyes JC, Muñoz FO, Ruiz JMG (2017). "Pautas de Disolución de Estromatolitos de Yeso en el Desierto de Atacama" [Dissolution Patterns of Gypsum Stromatolites in the Atacama Desert]. MACLA. **22**:33–34.

72. a, bBraissant O, Decho AW, Przekop KM, Gallagher KL, Glunk C, Dupraz C, Visscher PT (2009). "Characteristics and Turnover of Exopolymeric Substances in a Hypersaline Microbial Mat." FEMS Microbiol Ecol. **67**:293–307.

73. ^a, ^b*del Buey P, Sanz-Montero ME, Braissant O, Cabestrero Ó, Visscher PT (2021). "The Role of Microbial Extracellular Polymeric Substances on Formation of Sulfate Minerals and Fibrous Mg-Clays." Chem Geol. **581**:120403.*

74. ^*Cabestrero Ó, del Buey P, Sanz-Montero ME (2018b). "Biosedimentary and Geochemical Constraints on the Precipitation of Mineral Crusts in Shallow Sulphate Lakes." Sediment Geol. **366**:32–46.*

75. ^a, ^b*Van Driessche AE, Stawski TM, Kellermeier M (2019). "Calcium Sulfate Precipitation Pathways in Natural and Engineered Environments." Chem Geol. **530**:119274.*

76. ^*Zhang S, DePaolo DJ (2020). "Equilibrium Calcite-Fluid Sr/Ca Partition Coefficient from Marine Sediment and Pore Fluids." Geochim Cosmochim Acta. **289**:33–46.*

77. ^*Lv JJ, Ma F, Li FC, Zhang CH, Chen JN (2017). "Vaterite Induced by Lysinibacillus sp. GW-2 Strain and Its Stability." J Struct Biol. **200**:97–105.*

78. ^*del Buey P, Cabestrero Ó, Arroyo X, Sanz-Montero ME (2018). "Microbially Induced Palygorskite-Sepiolite Authigenesis in Modern Hypersaline Lakes (Central Spain)." Appl Clay Sci. **160**:9–21.*

Supplementary data: available at https://doi.org/10.32388/ED4EYH.3

Declarations

Funding: Proyecto CONICYT Postdoctorado 3190821, ANID National Doctoral Scholarship (No. 21181422) and Centro de Biotecnología “Profesor Alberto Ruiz” (CBAR-UCN). Additional support was provided to O.C. by MCIN/AEI/10.13039/5011000110033 under project PID2021-123735OB-C22/C21.

Potential competing interests: No potential competing interests to declare.